Redox Biology 48 (2021) 102171

Contents lists available at ScienceDirect

Redox Biology

journal homepage: www.elsevier.com/locate/redox

Metformin reduces macrophage HIF1α-dependent proinflammatory signaling to restore brown adipocyte function *in vitro*

Nuria Pescador [a,b,*], Vera Francisco [a], Patricia Vázquez [a,b], Eva María Esquinas [a], Cristina González-Páramos [a,c,d], M. Pilar Valdecantos [a,b], Irma García-Martínez [a,b], Andrés A. Urrutia [e], Laura Ruiz [a,b], Carmen Escalona-Garrido [a,b], Marc Foretz [f], Benoit Viollet [f], Miguel Ángel Fernández-Moreno [a,c,d], Alfonso L. Calle-Pascual [b,g,h], María Jesús Obregón [a], Julián Aragonés [e,i], Ángela M. Valverde [a,b,**]

[a] *Instituto de Investigaciones Biomédicas Alberto Sols (CSIC-UAM), Madrid, Spain*
[b] *Centro de Investigación Biomédica en Red de Diabetes y Enfermedades Metabólicas Asociadas (CIBERdem), Instituto de Salud Carlos III, Madrid, Spain*
[c] *Departamento de Bioquímica. Facultad de Medicina. Universidad Autónoma de Madrid, Spain and Instituto de Investigación Sanitaria Hospital 12 de Octubre (imas12), Madrid, Spain*
[d] *Centro de Investigación Biomédica en Red de Enfermedades Raras (CIBERer), Instituto de Salud Carlos III, Madrid, Spain*
[e] *Research Unit, Hospital de La Princesa, Instituto Investigación Sanitaria Princesa, Universidad Autónoma de Madrid, Spain*
[f] *Université de Paris, Institut Cochin, INSERM, CNRS, F-75014, Paris, France*
[g] *Departamento de Endocrinología y Nutrición, Hospital Clínico San Carlos, Instituto de Investigación Sanitaria Del Hospital Clínico San Carlos (IdISSC), Madrid, Spain*
[h] *Facultad de Medicina, Universidad Complutense de Madrid, Madrid, Spain*
[i] *Centro de Investigación Biomédica en Red de Enfermedades Cardiovasculares (CIBERcv), Instituto de Salud Carlos III, Madrid, Spain*

ARTICLE INFO

Keywords:
Brown adipose tissue
Obesity
Inflammation
Insulin resistance
Hypoxia-inducible factor-1α
Metformin

ABSTRACT

Therapeutic potential of metformin in obese/diabetic patients has been associated to its ability to combat insulin resistance. However, it remains largely unknown the signaling pathways involved and whether some cell types are particularly relevant for its beneficial effects. M1-activation of macrophages by bacterial lipopolysaccharide (LPS) promotes a paracrine activation of hypoxia-inducible factor-1α (HIF1α) in brown adipocytes which reduces insulin signaling and glucose uptake, as well as β-adrenergic sensitivity. Addition of metformin to M1-polarized macrophages blunted these signs of brown adipocyte dysfunction. At the molecular level, metformin inhibits an inflammatory program executed by HIF1α in macrophages by inducing its degradation through the inhibition of mitochondrial complex I activity, thereby reducing oxygen consumption in a reactive oxygen species (ROS)-independent manner. In obese mice, metformin reduced inflammatory features in brown adipose tissue (BAT) such as macrophage infiltration, proinflammatory signaling and gene expression, and restored the response to cold exposure. In conclusion, the impact of metformin on macrophages by suppressing a HIF1α-dependent proinflammatory program is likely responsible for a secondary beneficial effect on insulin-mediated glucose uptake and β-adrenergic responses in brown adipocytes.

1. Introduction

Since 1980 the global prevalence of overweight and obesity has been duplicated and currently almost one third of the world's population is affected by this pathology [1]. Obesity is characterized by a number of pathophysiological changes, including hypertrophy/hyperplasia of adipocytes, as well as chronic low-grade inflammation [2], both contributing to insulin resistance and related metabolic diseases such as type 2 diabetes (T2D) and cardiovascular diseases [3].

During the process of weight gain, the number of macrophages in

Abbreviations: BAT, brown adipose tissue; HIF1α, hypoxia-inducible factor-1α; T2D, type 2 diabetes; WAT, white adipose tissue; TNF, tumor necrosis factor; IL, interleukin; UCP1, uncoupling protein 1; HRE, hypoxia response elements; PHDs, prolyl hydroxylases; ROS, reactive oxygen species.

* Corresponding author. Instituto de Investigaciones Biomédicas Alberto Sols (CSIC-UAM), Madrid, Spain.
** Corresponding author. Instituto de Investigaciones Biomédicas Alberto Sols (CSIC-UAM), Madrid, Spain.
E-mail addresses: npescador@iib.uam.es (N. Pescador), avalverde@iib.uam.es (Á.M. Valverde).

https://doi.org/10.1016/j.redox.2021.102171
Received 20 September 2021; Received in revised form 13 October 2021; Accepted 15 October 2021
Available online 19 October 2021

white adipose tissue (WAT) is increased mainly by the recruitment of circulating monocytes shifting their polarity to a proinflammatory (M1) state. These macrophages secrete proinflammatory cytokines such as tumor necrosis factor (TNF) α, interleukin (IL) 1β and IL6 and increase the levels of the inducible nitric oxide synthase (iNOS) [2,4]. This inflammatory process and its deleterious impact on adipose cells' functionality has been mainly studied in WAT since, in the classical view, brown adipose tissue (BAT) [5,6] was thought to have limited physiological relevance in adult humans. However, in the last two decades imaging studies have identified metabolically active BAT depots in the interscapular and cervical areas of healthy adults [7–9]. Further research associates the amount of BAT with body mass index and other metabolic parameters such as fasting glucose, triglycerides, and cholesterol. Altogether, these seminal studies suggest that a decrease in active BAT may be associated with the accumulation of visceral WAT and unfavorable metabolic parameters [10,11]. Studies conducted in murine models of diet-induced obesity have shown infiltration of immune cells in BAT depots [12,13], one of them reporting reduced uncoupling protein 1 (UCP1) content [13].

Different processes have been proposed as triggers of the inflammatory state during obesity such as endoplasmic reticulum/oxidative stress and hypoxia of the adipose tissue [14–16]. The hypoxia-inducible factor HIF1α is responsible for regulating oxygen homeostasis [17]. During normoxia, HIF1α protein is degraded by prolyl hydroxylases (PHDs) through a mechanism involving the von Hippel-Lindau (VHL) protein in an ubiquitin- and proteasome-dependent manner [18]. HIF1α regulates the transcription of many genes involved in glucose and energy metabolism, iron metabolism, vascular development, cell proliferation, and viability [15,19]. Although PHDs are largely considered as direct oxygen sensors, some other studies have reported that accumulation of mitochondrial reactive oxygen species (ROS) can also mediate HIF1α stabilization in hypoxia [20–24]. In this line, it has been shown that ROS accumulation lead to inactivation of PHDs by promoting the oxidation of FeII into FeIII [25]. Moreover, it seems that this ROS-dependent HIF1α stabilization is particularly operative in hypoxia, but not in conditions close to anoxia [26].

Inflammation is another hypoxia-independent HIF1α stabilization condition [27,28] which has been attributed at least in part to the presence of an NFκB binding site in the proximal promotor of HIF1α [29]. Remarkably, genetic downregulation of HIF1α in adipocytes protects against inflammation and insulin resistance in obese mice [30–32]. On the other hand, Halberg et al. [30] reported that overexpression of a constitutively active form of HIF1α in adipocytes leads to weight gain and glucose intolerance, and indicates that aberrant HIF1α activity produces high local inflammation in WAT and an exacerbated diabetic phenotype. All these studies have shed light on the relevant role of HIF1α in developing obesity-associated inflammation and insulin resistance. However, the specific involvement of HIF1α in brown adipocytes and thermogenic BAT responsiveness during the inflammatory context of obesity has been less explored.

In this study we identified a molecular mechanism involving HIF1α in the negative impact of macrophages-mediated inflammation on brown adipocytes regarding their sensitivity to insulin and β-adrenergic responses. Since several pharmacological studies using metformin have revealed antiinflammatory properties of this antidiabetic drug [33–35], we also studied the effect of metformin in the interactome between macrophages and brown adipocytes, particularly related to HIF1α regulation.

2. Material and methods

Reagents and antibodies. Cell culture reagents were from Invitrogen (Carlsbad, CA, USA). Insulin (l0516), metformin (D150959) and CL316243 (C5976) were from Sigma (Sigma-Aldrich, Saint Louis, MO, USA). The anti-Large T antigen (LTAg) antibody was kindly provided by J. de Caprio (Dana Farber Cancer Institute, Boston, MA). Anti-phospho JNK (Thr 183/Tyr185) (#9251), anti-phospho STAT3 (Tyr705) (#9131), anti-phosho p38 MAPK (Thr180/Tyr182) (#9211), anti-p38 MAPK (#9212), anti-phospho Akt (Ser473) (#4058), anti-phospho Akt (Thr308) (#9275), anti-Akt (#9272), anti-phospho HSL (Ser660) (#4126), anti-HSL (#4107T), anti-phospho AMPK (Thr172) (#2531) and anti-AMPK (#2532) antibodies were from Cell Signaling Technology (MA, USA). Anti-GLUT4 (sc-53566), anti-GLUT1 (sc-1603), anti-JNK (sc-571), anti-iNOS (m19sc650) and anti-Vinculin (sc-73614) antibodies were from Santa Cruz (Palo Alto, CA, USA). Anti-IRS1 (06–248), anti-phospho IRS1 (Ser307) (07–247) and anti-AMPKα1 (07–350) antibodies were from Merck Millipore (Merck KGaA, Darmstadt, Germany). The anti-UCP1 antibody was purchased from Abcam (Ab109803, Cambridge, UK). The anti-HIF1α (10006421) antibody was from Cayman Chemical laboratories and the anti-F4/80 (MF 4F) antibody was from Immunostep (Salamanca, Spain).

Animals. Eight-week-old C75BL/6J male mice were purchased from Charles River. Mice were fed a HFD (60% of calories from fat, TD-06414, Envigo, Spain) for 10 weeks and then divided into two groups: mice that continued on a HFD for 6 additional weeks and mice fed a HFD and treated with metformin hydrochloride (100 mg/kg) daily by oral gavage. Then, half of the mice of each group were exposed to the cold (4 °C) for 16 h. Animal experimentation was approved by the Ethics Committees of Consejo Superior de Investigaciones Científicas and Comunidad de Madrid (Spain) in accordance with the European Union guidelines.

Generation of brown preadipocyte cell lines and differentiation. Brown preadipocytes were isolated from the interscapular BAT of 20-day old suckling mice and immortalized as previously described [36]. Brown preadipocytes were also immortalized from *Ampkα1*$^{-/-}$ mice [37] or mice containing loxP-flanked alleles of HIF1α previously described [38], referred as BA$^{Ampk\alpha1-/-}$ and BA$^{Hif1afl/fl}$, respectively.

For differentiation, immortalized brown preadipocytes were grown in DMEM supplemented with 10% fetal bovine serum (FBS), 20 nM insulin and 1 nM triiodothyronine (T3) (differentiation medium, DM) until reaching confluence. Next, the cells were cultured for 2 days in induction medium (IM) consisting of DM supplemented with 0.5 μM dexamethasone, 0.125 μM indomethacin, 1 μM rosiglitazone and 0.5 mM isobutyl-methyl-xanthine (IBMX). Then, cells were cultured in DM until day 7 in which they exhibited a fully differentiated phenotype.

To generate *Hif1α* null brown adipocytes (BA$^{Hif1a\Delta/\Delta}$), at day 6 of differentiation BA$^{Hif1afl/fl}$ were transduced with adenoviruses encoding cre recombinase or β galactosidase at a titer of 4 x 10^{10} plaque-forming units. After 48 h (day 8), cells were used for experiments.

To generate a brown adipocyte cell line stably expressing HIF1α, we used the retroviral vector pRv-HIF1a(P2)* encoding a mutated version of HIF1α at positions P402 and P564 which lacks critical proline residues and is therefore not recognized by VHL [39]. This construct is constitutively active under normoxic conditions irrespective of the oxygen tension [40]. As a control, we utilized the empty vector pRv. For retroviral infection, Phoenix cells seeded in p100 culture dishes were transfected with 10 μg of each retroviral vector and 10 μg of the pCLAmpho Retrovirus Packaging Vector (Imgenex) using Lipofectamine 2000 (Invitrogen). Cell culture supernatants were harvested 24 h after transfection, filtered through a 0.45-μm filter, diluted (1:2) with fresh medium containing 8 mg/ml polybrene (Sequabrene, Sigma) and preadipocytes were differentiated until day 7.

Isolation and culture of bone marrow derived macrophages (BMDM). BMDM were obtained by flushing bone marrow from 8 weeks-old C57BL/6J mice femurs and tibias. Briefly, mice were euthanized by CO_2 inhalation and death was ensured by cervical dislocation. The skin of the mouse was disinfected with 70% alcohol. The tibia and femur were isolated and any tissue was removed from the bones. The epiphyses were cut of the bones and flushed the marrow into a 50 ml centrifuge tube using a 5 ml syringe and a 25G needle. The cell suspension was filtered with a 75 μm cell strainer in a new 50 ml tube to remove the excess of tissue, fat or other debris (all this procedure was performed

under a laminar flow hood). Cell suspension was centrifuged at 300 × g for 5 min and the pellet was resuspended in 2 ml of ACK lysis buffer for 2 min at RT to lysate the red blood cells. Cells were washed with complete DMEM medium and centrifuged at 300 × g for 5 min. Then, bone marrow cells were cultured with L929 differentiation medium (10% FBS, 1% P/S, 10–30% of L929-CM) in non-treated p100 plates for 6–8 days to differentiate into macrophages.

Generation of conditioned media in macrophages and treatment of brown adipocytes. Raw 246.7 murine macrophages cell line and BMDM were used to obtain conditioned media for the *in vitro* experiments. Raw 246.7 macrophages were cultured in Roswell Park Memorial Institute (RPMI) 1640 medium supplemented with 10% heat-inactivated FBS, antibiotics (1% P/S; 100 U/ml penicillin, 100 μg/ml streptomycin) and glutamine (2 mM) at 37 °C in a humidified atmosphere with 5% CO_2. To generate a proinflammatory CM (CM-Lps), confluent (90–95%) macrophages were treated for 4 h with 100 ng/ml LPS (InvivoGen, California, USA) in RPMI medium supplemented with 2% FBS, 1% P/S and 2 mM glutamine. Then, cells were washed twice with phosphate buffer saline (PBS) and kept in RPMI-2% FBS for 16 h. To obtain an antiinflammatory CM (CM-LpsMet), confluent Raw 246.7 macrophages were treated with 100 ng/ml LPS as detailed above and then the cells were washed twice with PBS and treated with metformin (10 mM) in RPMI medium-2% FBS for 16 h. To produce CM from Raw 246.7 macrophages with inhibited complex I activity (CM-LpsRtn), cells were treated with 100 ng/ml LPS as detailed above and then the cells were treated with rotenone (1 μM) for 2 h after which they were washed twice with PBS and maintained in RPMI-2% FBS for a further 16 h. To produce CM from macrophages with inhibited HIF1α transcriptional activity (CM-InhLps), Raw 246.7 cells were pretreated with a transcriptional inhibitor of HIF1α (sc-205346, Santa Cruz) at 30 μM concentration in RPMI-2% FBS, 1% P/S and 2 mM glutamine for 1 h. Then, LPS (100 ng/ml LPS) was added for 4 h in the presence of the HIF1α inhibitor. After this time, the cells were washed twice with PBS and maintained in RPMI-2% FBS for a further 16 h. As control, CM was collected from macrophages maintained for the corresponding time-periods in RPMI-2% FBS (referred as CM-Ctl). Similar treatment to generate CM was conducted in BMDM using 150 ng/ml LPS and 1 mM metformin, dose previously used to treat BMDM [41]. Before addition to brown adipocytes, all CM were harvested and filtered through a 0.22-μm filter to remove cell debris.

Measurement of nitrite production. NO production was evaluated in the CM by measuring nitrites, an oxidative product of NO. Nitrite content was determined by the Griess reaction [42]. Aliquots of CM were collected and mixed with 1 mM sulphanilic acid (151057.1208, Panreac) and 1 mM N-(l-naphthyl) ethylenediamine (NEDA) (N912510G, Sigma-Aldrich). Nitrites production was measured spectrophotometrically at 548 nM and the concentration was determined by a standard curve of NO_2.

Conditioned medium cytokine detection assay. CM were collected and immediately frozen at −80 °C. TNFα, IL6 and IL1β were determined using Luminex 100 IS (Merck Millipore, Darmstadt, Germany).

Treatment of differentiated brown adipocytes with CM. For experiments, differentiated brown adipocytes were treated with CM-Lps, CM-LpsMet, CM-LpsRtn, CM-InhLps or the corresponding CM-Ctl for several time-periods to analyze proinflammatory signaling cascades. For insulin signaling, brown adipocytes were pretreated with either CM for 16 h prior to stimulation with 10 nM insulin (Sigma-Aldrich, Missouri, USA) for 10 min. To study β-adrenergic responses, brown adipocytes were treated with either CM in the presence of 2 μM CL316243 for several time-periods as described in results and figure legends. At the end of the treatment cells were washed twice with PBS and collected for further analysis.

Treatment of brown adipocytes with cytokines. Differentiated brown adipocytes were treated with a cocktail of TNFα (300-01A, PeproTech), IL6 (216–16, PeproTech) and IL1β (211-11B, PeproTech) (30 ng/ml each) for 16 h in serum-free RPMI medium. Responses to insulin and CL316243 were determined as described for the treatment with CM.

Measurement of glucose uptake. Differentiated brown adipocytes were treated with CM-Ctl or CM-Lps for 16 h and after cells were serum-deprived for 1 h. Then, cells were washed with ice-cold Krebs-Ringer-phosphate buffer (KRP) (135 mM NaCl, 5.4 mM KCl, 1.4 mM $CaCl_2$, 1.4 mM $MgSO_4$, 10 mM sodium pyrophosphate, pH 7.4) and incubated with KRP buffer with or without insulin for 10 min at 37 °C. Then, 2-Deoxy-D [1–^{3}H] glucose (500 nCi/ml) was added to this solution, and the incubation was continued for 5 min at 37 °C. The cells were washed with ice-cold KRP buffer and solubilized with a syringe in 1% SDS as previously described [43]. After 2 h incubation at 37 °C, radioactivity was measured by liquid scintillation counting. Total protein was determined by BCA method and results were normalized to the protein amount of each culture plate.

Measurement of glycerol release. After treatment of brown adipocytes with 2 μM CL316243 for 3 h, cell medium was removed and glycerol content was measured using a commercial kit (Biosystems, Barcelona, Spain) according to the manufacturer's instructions.

Homogenization and preparation of tissue extracts. Frozen BAT samples were homogenized in 16 vol (w/v) of ice-cold lysis buffer containing 50 mM Tris-HCl, 1% Triton X-100, 2 mM EGTA, 10 mM EDTA, 100 mM NaF, 1 mM Na_4P2O_7, 2 mM Na_3VO_4, 100 μg/ml phenylmethylsulphonyl fluoride (PMSF), 1 μg/ml aprotinin, 1 μg/ml pepstatin A and 1 μg/ml leupeptin. Samples were homogenized in the same lysis buffer using the Brinkman PT 10/35 Polytron. Extracts were kept ice-cold at all times. Tissue extracts were cleared by centrifugation at 40,000×*g* for 20 min at 4 °C twice. The supernatant was aliquoted and stored at −80 °C.

Preparation of protein cell extracts and Western blot. Cells were scraped off in ice-cold PBS, pelleted by centrifugation at 4000×*g* for 10 min at 4 °C and resuspended in buffer containing 10 mM Tris-HCl, 5 mM EDTA, 50 mM NaCl, 30 mM disodium pyrophosphate, 50 mM NaF, 100 μM Na_3VO_4, 1% Triton X-100, 1 mM PMSF, 10 μg/ml leupeptin and 10 μg/ml aprotinin pH 7.6 (lysis buffer). Cell lysates were clarified by centrifugation at 12,000×*g* for 10 min at 4 °C twice. Protein content was determined by the Bradford method, using the Bio-Rad reagent and bovine serum albumin (BSA) as the standard. After SDS-PAGE, proteins were transferred to Immobilon membranes (Merk-Millipore), blocked using 5% non-fat dried milk or 3% BSA in 10 mM Tris-HCl, 150 mM NaCl pH 7.5, and incubated overnight with the antibodies indicated in 0.05% Tween-20, 10 mM Tris-HCl, 150 mM NaCl pH 7.5. Immunoreactive bands were visualized using the ECL Western blotting protocol (Merk-Millipore).

Quantitative real-time PCR (RT-qPCR). Total RNA was extracted with Trizol (Invitrogen). Complementary DNA (cDNA) was synthesized by reverse transcription PCR (RT-PCR) from 1 μg of RNA using SuperScript™ III First-Strand Synthesis System for quantitative PCR (qPCR) following the manufacturer's indications (Invitrogen). RT-qPCR was performed with an ABI 7900 sequence detector (Applied Biosystems).

Lipid staining. To visualize lipid droplets in brown adipocytes, BODIPY 493/503 stock solution (1 mg/ml in methanol) (d-3922; Molecular Probes) was diluted 1:1000 in RPMI medium supplemented with 2% FBS before addition to differentiated brown adipocytes for 30 min. Then, cells were fixed with 4%-PFA. Mounting medium (Vectashield with 4,6-diamidino-2-phenylindole (DAPI), H-1200, Vector Laboratories) was used for fluorescence imaging. Brown adipocytes were observed and images were captured using an LSM 700 confocal microscope (Zeiss).

Immunofluorescence analysis in brown adipocytes. Brown preadipocytes were differentiated on glass coverslips, fixed in 4%-paraformaldehyde (PFA) and processed for immunofluorescence. Briefly, anti-GLUT4 (sc-56566, Santa Cruz) or anti-GLUT1 (sc-377,228, Santa Cruz) primary antibodies were applied for 1 h at 37 °C in PBS-1% BSA at 1/50 dilution. The secondary antibody used was Alexa 488 goat anti-mouse (Invitrogen) at 1/500 dilution. Cell nuclei were counterstained with DAPI (Sigma). Immunofluorescence was examined using an LSM

700 confocal microscope (Zeiss).

Histological analysis and immunostaining. For immunohistochemistry, BAT tissue was fixed in 4%-PFA (16,005, Sigma-Aldrich) for 24 h, washed twice with PBS, dehydrated with ascending ethanol solutions, incubated with xylene, and then embedded in paraffin. Blocks were cut into 5 μm sections. Prior to H&E staining or immunohistochemistry, the sections were deparaffinized in xylene and hydrated in descending ethanol solutions and distilled water. The slides were stained with Mayer's hematoxylin (MHS32-1L, Sigma-Aldrich) for 15–20 min and eosin (1.15935.0025, Merck) for 1 min. After, the slides were dried and mounted and the images were captured with an Axiophot light microscope (Zeiss) using a 40 × objective.

For UCP1 and HIF1α immunohistochemistry, sections were heated for 20 min in 100 mM sodium citrate buffer (pH 6.0) and 0.05% Tween-20. After washing with PBS, endogenous peroxidase was blocked by incubation with a solution of 9% H_2O_2 in 10% methanol for 10 min at RT. The tissue sections were then incubated in 6% BSA and 2% normal horse serum (NHS) in PBS-0.1% Triton X-100 for 1 h at room temperature to block non-specific binding. The sections were incubated with primary antibody against UCP1 (1:500, Ab10983, Abcam) or primary antibody against HIF1α (1:100, anti HIF-1α Rat monoclonal antibody (SIMA343B) kindly donated by Dr. Martín-Puig from Centro Nacional de Investigaciones Cardiovasculares, CNIC & Universidad Francisco de Vitoria, Madrid, Spain) overnight at 4 °C. Sections were then washed with PBS and incubated with biotinylated secondary anti-rabbit (1:250) (BA-1100, Vector Laboratories) in the case of UCP1 or biotinylated secondary anti-rat (1:250) (BA-4000, Vector Laboratories) for HIF1α for 1 h at room temperature. After washing with PBS, the slides were incubated with DAB-immunoperoxidase staining (SK-4100, Vector Laboratories). After washing with water for 5 min, the sections were counterstained with hematoxylin (H3136, Sigma-Aldrich) solution for 10 s and rinsed again with water. After dehydration and xylene incubation, the sections were assembled with DePeX (18243.02, SERVA Electrophoresis GmbH), covered with coverslips, and dried overnight.

For immunofluorescence staining of BAT, paraffin sections were deparaffinized and rehydrated. The sections were boiled in 10 nM citrate buffer for 5 min and treated with 0.3% Triton X-100 in PBS for 10 min. Then, the sections were blocked with 0.3% Triton X-100 in PBS containing 0.5% BSA for 1 h at room temperature. Thereafter, sections were incubated with blocking solution containing primary antibodies (1:250, anti-HIF1α Rat monoclonal antibody (SIMA343B) or 1:500, anti F4/80, Immunostep) overnight at 4 °C. Finally, the sections were washed and probed with Alexa-conjugated secondary antibodies. Fluorescent images were taken with the confocal microscope.

MitoTracker Green and MitoSOX Red labelling. Raw 264.7 cells were loaded with 100 nM green-fluorescent MitoTracker Green (MitoGreen, Invitrogen, M7514) for 30 min at 37 °C to measure mitochondrial content, followed by a wash with warmed complete culture medium. To examine mitochondrial reactive oxygen species (ROS) levels, cells were loaded with 5 μM MitoSOX Red (MitoSOX, Invitrogen, M36008) for 30 min at 37 °C, which is a mitochondrial superoxide indicator. Quantification of fluorescence intensity was carried out by using a BD LSR II flow cytometer (Becton Dickinson, Franklin Lakes, NJ, USA) with at least 10,000 events for each sample and analyzed with Becton Dickinson FACS Diva (version 6.1.2).

Oxygen consumption measurements. Raw 264.7 cells were treated with 100 ng/ml LPS for 4 h and then treated with or without 10 mM metformin for 16 h. The average intracellular oxygen consumption rate (OCR) was measured in a sealed chamber using a Clark-type S1 electrode (Oxygraph System, Hansatech Instruments) according to the manufacturer's instructions, as described [44].

Seahorse analysis. Mitochondrial function was evaluated with a Seahorse XF24 analyzer (Agilent, CA, USA). Raw 246.7 macrophages were seeded at a density of 8×10^4 cells/well in XF-24 plates in RPMI medium supplemented with 10% heat-inactivated FBS, antibiotics (1% P/S; 100 U/ml penicillin, 100 μg/ml streptomycin) and glutamine (2 mM). The following day, cells were treated with LPS without or with metformin as described above. Briefly, culture medium was replaced with 500 μl RPMI supplemented with 1 mM HEPES, 1 mM sodium pyruvate, and 2 mM L-glutamine, and the plates were equilibrated in a non-CO_2 incubator at 37 °C. Metabolic toxins (0.5 μM oligomycin, 1 μM carbonyl cyanide *p*-trifluoromethoxy-phenylhydrazone [FCCP], 0.5 μM rotenone and antimycin A [Rot/AA]) were loaded into the cartridge drug ports. The cellular oxygen consumption rate (OCR) was measured in real-time by adding the drugs in order according to the manufacturer's protocol.

Determination of mitochondrial complex I activity. The activity of the respiratory chain complex I was measured as previously described [45] using a Beckman Coulter DU 800 spectrophotometer.

Quantification and statistical analysis. Statistical details of the experiments including statistical tests used, exact value of n, dispersion and precision measures (mean ± SEM), and statistical significance are reported in the Figures and Figure Legends. The differences between 2 groups with similar variances were analyzed using a two-tailed Student's *t*-test. When the variances of the groups were significantly different, a two-tailed *t*-test with Welch's correction was used. Differences between the variances of the groups were analyzed with the Fisher test (F-test). When more than 2 groups were analyzed, statistical analysis was performed by one-way ANOVA followed by Tukey's post hoc test. All statistical analyses were performed using GraphPad Prism 8 software. A *p* value lower than 0.05 was considered significant.

3. Results

Metformin reduces macrophage-mediated proinflammatory signaling cascades in brown adipocytes. Metformin is a widely prescribed drug for T2D that besides its well-known effects in insulin-sensitive tissues also reduces the proinflammatory responses of macrophages [33,46,47]. Based on that, we investigated the effect of metformin in the crosstalk between macrophages and brown adipocytes in the context of inflammation. To achieve this, we collected conditioned media from M1 (LPS-stimulated) Raw 264.7 macrophages without or with a further treatment with metformin (referred to as CM-Lps or CM-LpsMet, respectively) as detailed in Materials and Methods. As control, CM was collected from macrophages that did not receive treatment (CM-Ctl). Quantification of proinflammatory cytokines in the CM (Table S1) revealed a significant decrease in TNFα and IL6 content in the CM-LpsMet compared to levels detected in CM-Lps. Next, activation of proinflammatory signaling cascades was tested in brown adipocytes exposed to the different CM. As shown in Fig. 1, STAT3, JNK, and p38 MAPK phosphorylation was rapidly detected in brown adipocytes stimulated with CM-Lps, an effect that concurred with the degradation of IκBα. Notably, activation of proinflammatory signaling was markedly attenuated in brown adipocytes treated with CM-LpsMet.

CM-LpsMet prevented the impairment in insulin signaling in brown adipocytes induced by CM-Lps. Several studies have demonstrated that activation of proinflammatory signaling cascades interferes with the early steps of insulin signaling by phosphorylating IRS1 at serine residues, thereby triggering its degradation via 26S proteasome [48,49]. In this regard, we previously reported that cytokines secreted by M1-polarized macrophages induced insulin resistance in hepatocytes [50]. As depicted in Fig. 2A, stimulation of brown adipocytes with CM-Lps led to a rapid and transient phosphorylation of IRS1 at serine 307 peaking at 30 min and declining after that. This effect concurred with a marked reduction in IRS1 protein levels 24 h after treatment with the proinflammatory CM-Lps (Fig. 2B). Both IRS1 serine 307 phosphorylation at its subsequent degradation were abolished in brown adipocytes receiving CM-LpsMet (Fig. 2A and B). To monitor insulin responses downstream of IRS1, CM-Lps, CM-LpsMet or CM-Ctl were added to brown adipocytes for 24 h and then, cells were stimulated with 10 nM insulin for a further 10 min. Fig. 2C shows a substantial decrease in insulin-induced Akt phosphorylation at both serine 473 and threonine

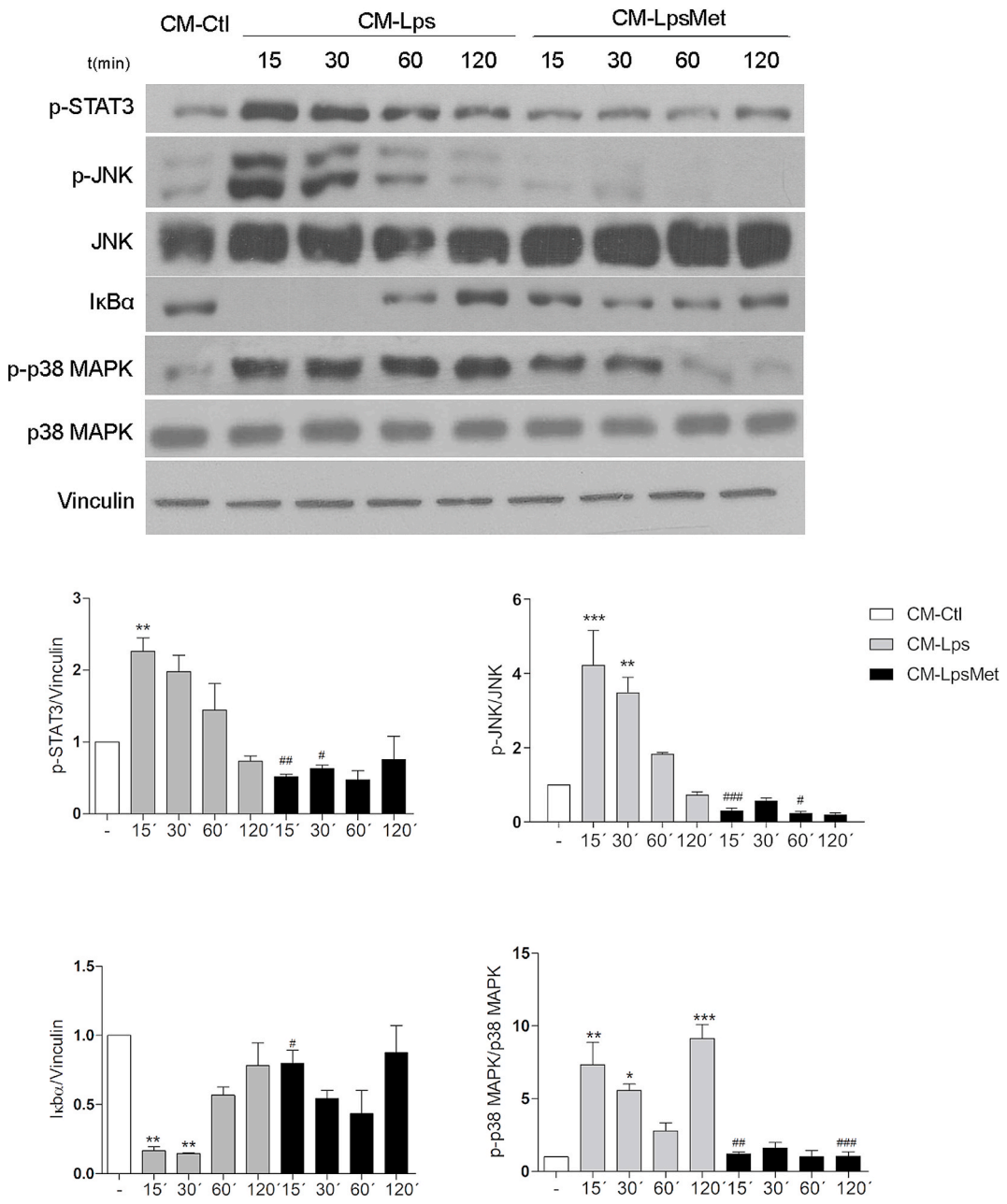

Fig. 1. *Metformin attenuates macrophage-mediated proinflammatory signaling cascades in brown adipocytes.* Differentiated brown adipocytes were treated with CM-Ctl, CM-Lps, or CM-LpsMet for the indicated time-periods. Representative Western blots of phospho-STAT3, phospho-JNK, JNK, IκBα, phospho-p38 MAPK, p38 MAPK, and Vinculin levels and quantification (n = 3 independent experiments). Results are expressed as fold change versus CM-Ctl condition. *p < 0.05, **p < 0.01, ***p < 0.001 versus CM-Ctl; #p < 0.05, ##p < 0.01, ###p < 0.001 versus CM-Lps with one-way ANOVA followed by Tukey's post hoc.

308 residues in brown adipocytes preincubated with CM-Lps compared to those treated with CM-Ctl or CM-LpsMet. Similar effect of the CM-Lps in decreasing IRS1 and insulin-induced Akt phosphorylation in brown adipocytes and the CM-LpsMet in preventing these responses was found when the CM was generated in BMDM (Fig. S1A).

Since insulin induces glucose uptake in brown adipocytes in a PI-3-kinase/Akt-dependent manner [6], we assessed the effect of the inflammatory environment and metformin in this response. Whereas almost a three-fold increase in glucose uptake was found in insulin-stimulated brown adipocytes upon pretreatment with CM-Ctl, this effect was markedly attenuated in cells pretreated with CM-Lps (Fig. 2D) and correlated with a decrease in GLUT4 translocation to the plasma membrane (Fig. 2E). Of note, CM-Lps increased basal (insulin-independent) glucose uptake (Fig. 2D) in parallel with an increase in *Glut1* (*Slc2a1*) mRNA levels and GLUT1 immunostaining (Fig. 2F and G) resulting in only about 1.4-fold increase in insulin-dependent glucose uptake. Brown adipocytes treated with CM-LpsMet did not show impairments in insulin-induced glucose uptake and GLUT4 translocation to the plasma membrane and also GLUT1 up-regulation was not observed. Importantly, in these cells the increase in insulin-dependent glucose uptake was comparable to the controls (Fig. 2D, E, 2F, 2G).

CM-Lps, but not CM-LpsMet, decreased β-adrenergic-mediated lipolysis and UCP1 levels in brown adipocytes. The impact of inflammation was evaluated in β-adrenergic stimulated lipolysis as an early trigger of brown adipocyte thermogenic response. Brown adipocytes were stimulated with the β3-adrenergic agonist CL316243 (2 μM) for 3 h in the presence of CM-Lps, CM-LpsMet or CM-Ctl. Fig. 3A shows that cells treated with CM-Ctl were sensitive to CL316243 manifested by

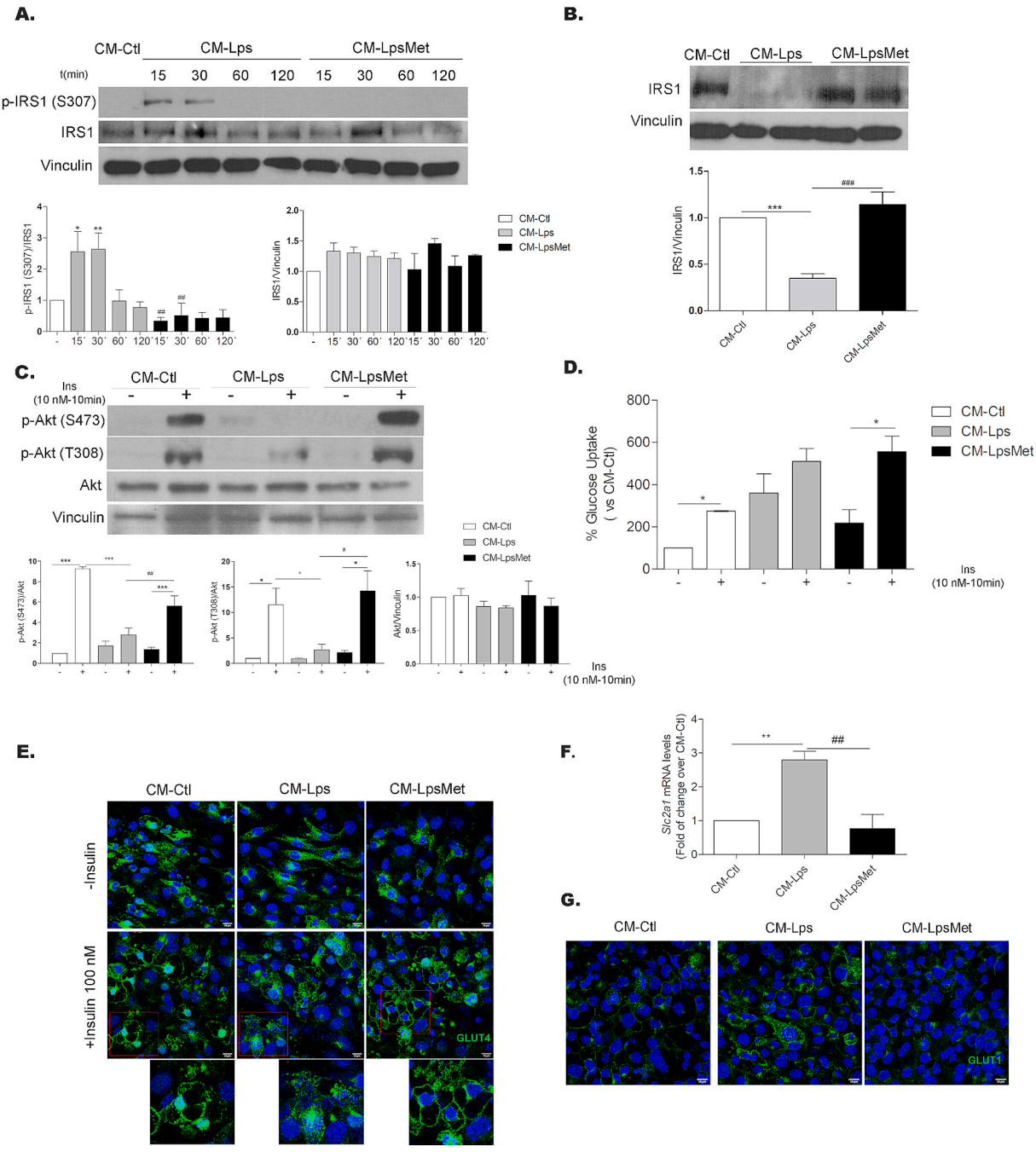

Fig. 2. *The impairment of insulin signaling in brown adipocytes treated with CM-Lps was prevented in brown adipocytes exposed to CM-LpsMet.* **A)** Differentiated brown adipocytes were treated with CM-Ctl, CM-Lps or CM-LpsMet for the indicated time-periods. Representative Western blot of phospho-IRS1 (Ser307), IRS1 and Vinculin protein levels and quantification (n = 3 independent experiments). Results are expressed as fold change versus CM-Ctl. *p < 0.05, **p < 0.01 versus CM-Ctl; $^{\#\#}$p < 0.01 versus CM-Lps. **B)** IRS1 and Vinculin levels in brown adipocytes treated with CM-Ctl, CM-Lps or CM-LpsMet for 24 h and quantification (n = 3 independent experiments). ***p < 0.001 versus CM-Ctl; $^{\#\#\#}$p < 0.001 versus CM-Lps. **C)** Differentiated brown adipocytes were treated with CM-Ctl, CM-Lps or CM-LpsMet for 24 h followed by stimulation with 10 nM insulin for 10 min. Representative Western blots using the indicated antibodies and respective quantification (n = 4 independent experiments). *p < 0.05, ***p < 0.001 versus without insulin; $^{+}$p<0.05, $^{+++}$p<0.001 versus CM-Ctl; $^{\#}$p < 0.05, $^{\#\#}$p < 0.01 versus CM-Lps. **D)** Glucose uptake under conditions described in C (n = 3 independent experiments performed in duplicate). *p < 0.05 versus without insulin. **E)** Representative GLUT4 immunofluorescence images in differentiated brown adipocytes treated with CM-Ctl, CM-Lps or CM-LpsMet for 18 h followed by stimulation with 100 nM insulin for 10 min (nuclei in blue (DAPI), GLUT4 in green). Scale bars, 10 μm. **F)** mRNA levels of *Slc2a1* after 18 h of treatment with CM-Ctl, CM-Lps or CM-LpsMet (n = 4 independent experiments performed in duplicate). **p < 0.01 versus CM-Ctl; $^{\#\#}$p < 0.01 versus CM-Lps. **G)** Representative GLUT1 immunofluorescence images of differentiated brown adipocytes treated with CM-Ctl, CM-Lps or CM-LpsMet for 18 h (nuclei in blue (DAPI), GLUT1 in green). Scale bars, 10 μm. Data are shown as mean ± SEM. Statistical analysis was performed using two-tailed unpaired *t*-test when comparing two groups and one-way ANOVA followed by Tukey's post hoc test when comparing three or more groups. (For interpretation of the references to colour in this figure legend, the reader is referred to the Web version of this article.)

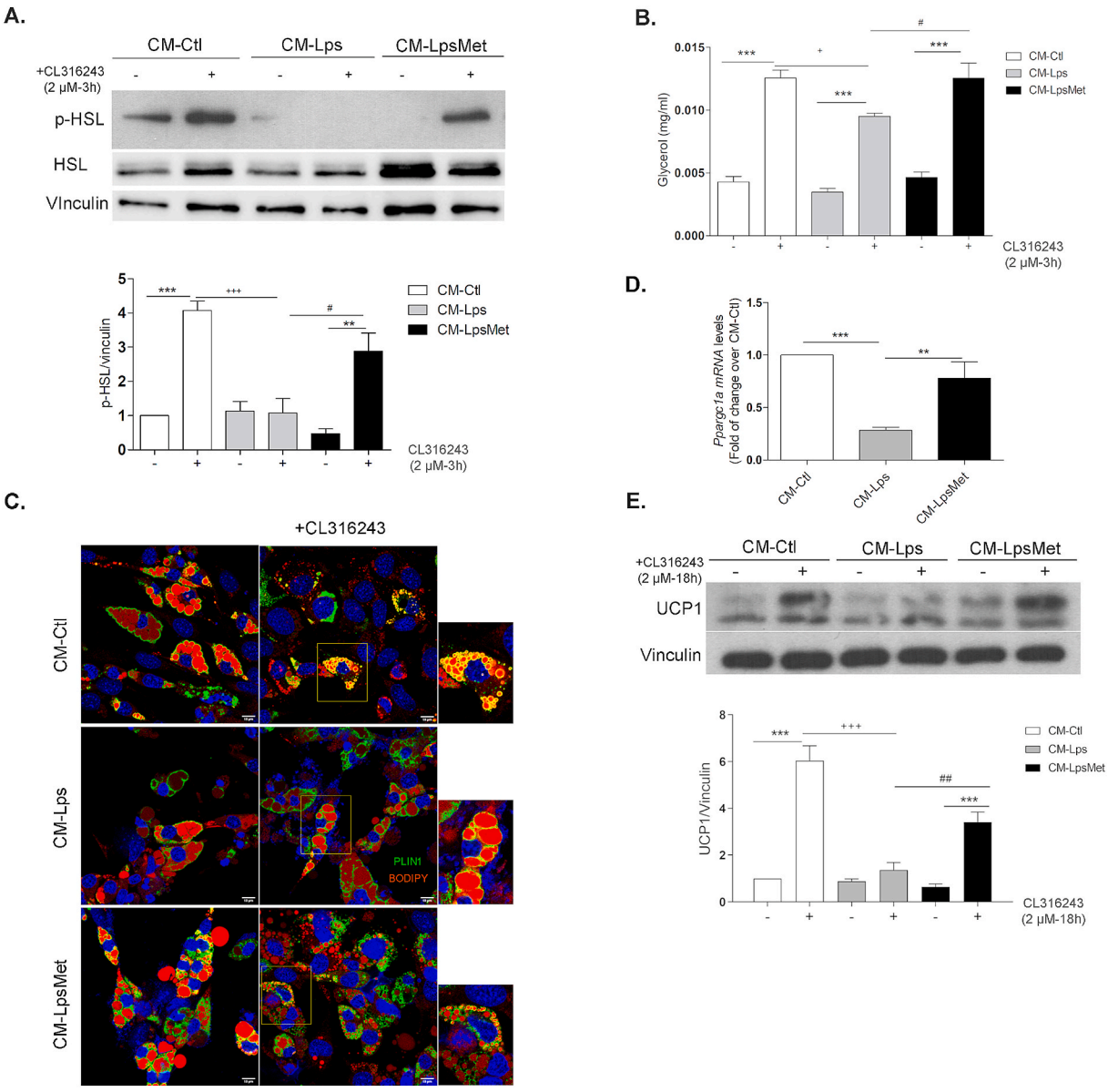

Fig. 3. *CM-Lps, but not CM-LpsMet, decreased β3-adrenergic-mediated lipolysis and UCP1 levels in brown adipocytes.* **A)** Representative Western blots of phospho-HSL, HSL and Vinculin levels and quantification in differentiated brown adipocytes treated with CM-Ctl, CM-Lps or CM-LpsMet for 18 h followed by stimulation with 2 μM CL316243 for the last 3 h (n = 6 independent experiments). Results are expressed as fold change versus CM-Ctl. **B)** Glycerol released to the culture medium was measured as described in Materials and Methods (n = 4 independent experiments performed in triplicate). ***p < 0.001 versus without CL316243; $^{+}$p<0.05 versus CM-Ctl with CL316243; $^{\#}$p < 0.05 versus CM-Lps with CL316243. **C)** Representative images of immunofluorescence of PLIN1 (green) in differentiated brown adipocytes upon treatment with CM-Ctl, CM-Lps or CM-LpsMet for 24 h and CL316243 (2 μM) during the last 8 h. BODIPY 493/503 staining before fixation is shown in red. Scale bars, 10 μm. **D)** mRNA levels of *Ppargc1a* in differentiated brown adipocytes treated with CM-Ctl, CM-Lps or CM-LpsMet for 18 h (n = 4 independent experiments performed in duplicate). ***p < 0.001 versus CM-Ctl; $^{\#\#}$p < 0.01 versus CM-Lps. **E)** Representative Western blot images of UCP1 and Vinculin levels and quantification in brown adipocytes stimulated with 2 μM CL316243 in the presence of CM-Ctl, CM-Lps or CM-LpsMet for 18 h (n = 5 independent experiments). ***p < 0.001 versus without CL316243; $^{+++}$p<0.001 versus CM-Ctl + CL316243; $^{\#\#}$p < 0.01 versus CM-Lps + CL316243. Data are shown as mean ± SEM. Statistical was performed using one-way ANOVA followed by Tukey's post hoc test. (For interpretation of the references to colour in this figure legend, the reader is referred to the Web version of this article.)

hormone-sensitive lipase (HSL) phosphorylation and, consequently, the release of glycerol to the culture medium (Fig. 3B). Both responses were significantly altered in brown adipocytes treated with CL316243 and CM-Lps, but not CM-LpsMet. We also analyzed the effect of the proinflammatory environment in lipolysis by performing PLIN1 (Perilipin 1) immunofluorescence and Bodipy staining. As shown in Fig. 3C, smaller lipid droplets surrounded by PLIN1 were found in brown adipocytes co-treated with CL316243 and CM-Ctl. In cells exposed to CM-Lps and CL316243 lipid droplet size was similar to those of unstimulated cells. However, in the presence of CM-LpsMet, brown adipocytes maintained their β3-adrenergic lipolytic response manifested by the smaller size of their lipid droplets. The reduced sensitivity of brown adipocytes to β3-adrenergic stimulation by the CM-Lps and the protection by CM-LpsMet was also evident in *Ppargc1a* (encoding PGC1α) mRNA levels and UCP1 protein content (Fig. 3D and E). As occurred with the insulin response, the effect of the CM-Lps in decreasing CL316243-mediated UCP1 expression and the protective effect of CM-LpsMet was found in brown adipocytes exposed to the CM generated by BMDM (Fig. S1B).

Treatment of obese mice with metformin reduced BAT inflammation and increased cold responsiveness. We aimed to provide a

physiological relevance to the *in vitro* findings in obese C57BL/6J mice treated or not with a daily dose of metformin (100 mg/kg) for 6 weeks. Treatment of obese mice with metformin reduced glucose levels and body weight (Fig. S2). As shown in Fig. 4A, metformin administration decreased the phosphorylation of STAT3, JNK and IκB, all readouts of proinflammatory signaling, in BAT. Likewise, treatment with metformin reduced *Il6* and *Il1b* mRNA levels in BAT from obese mice (Fig. 4B), revealing a decrease in tissue inflammation. A step further, in a cohort of mice exposed to 4 °C (CE) for 6 h, *Ppargc1a* and *Ucp1* mRNA levels were elevated in BAT to a higher extend in mice that received metformin prior to cold exposure (Fig. 4C and D). This effect was confirmed by UCP1 immunohistochemistry in BAT sections (Fig. 4E).

Stabilization of HIF1α is sufficient and necessary to decrease β-adrenergic responses in brown adipocytes. Due to the existence of a direct relationship between hypoxia and inflammation at the level of HIF1α-mediated transcriptional regulation of proinflammatory mediators [51,52], we tested whether HIF1α was stabilized in brown adipocytes upon treatment with the proinflammatory CM-Lps. Fig. 5A shows HIF1α stabilization in brown adipocytes treated with CM-Lps, an effect markedly attenuated in cells receiving CM-LpsMet. Likewise, expression levels of the proinflammatory markers *Tnfa*, *Il6*, *Il1b* and *Nos2* were elevated in brown adipocytes exposed to CM-Lps, pointing to a secondary inflammatory response in brown adipocytes that significantly decreased in those receiving CM-LpsMet. Increased HIF1α immunostaining was detected in the nucleus of both brown adipocytes (rounded) and immune cells (smaller and enlarged) in BAT sections from obese mice (Fig. 5B) and, importantly, these two different nuclear HIF1α signals were not detected in metformin-treated mice. These results prompted us to hypothesize that stabilization of HIF1α in differentiated brown adipocytes could mimic the impairment of insulin and β-adrenergic responses of the proinflammatory CM-Lps. To test this, brown adipocytes were transduced with retroviral particles expressing a HIF1α

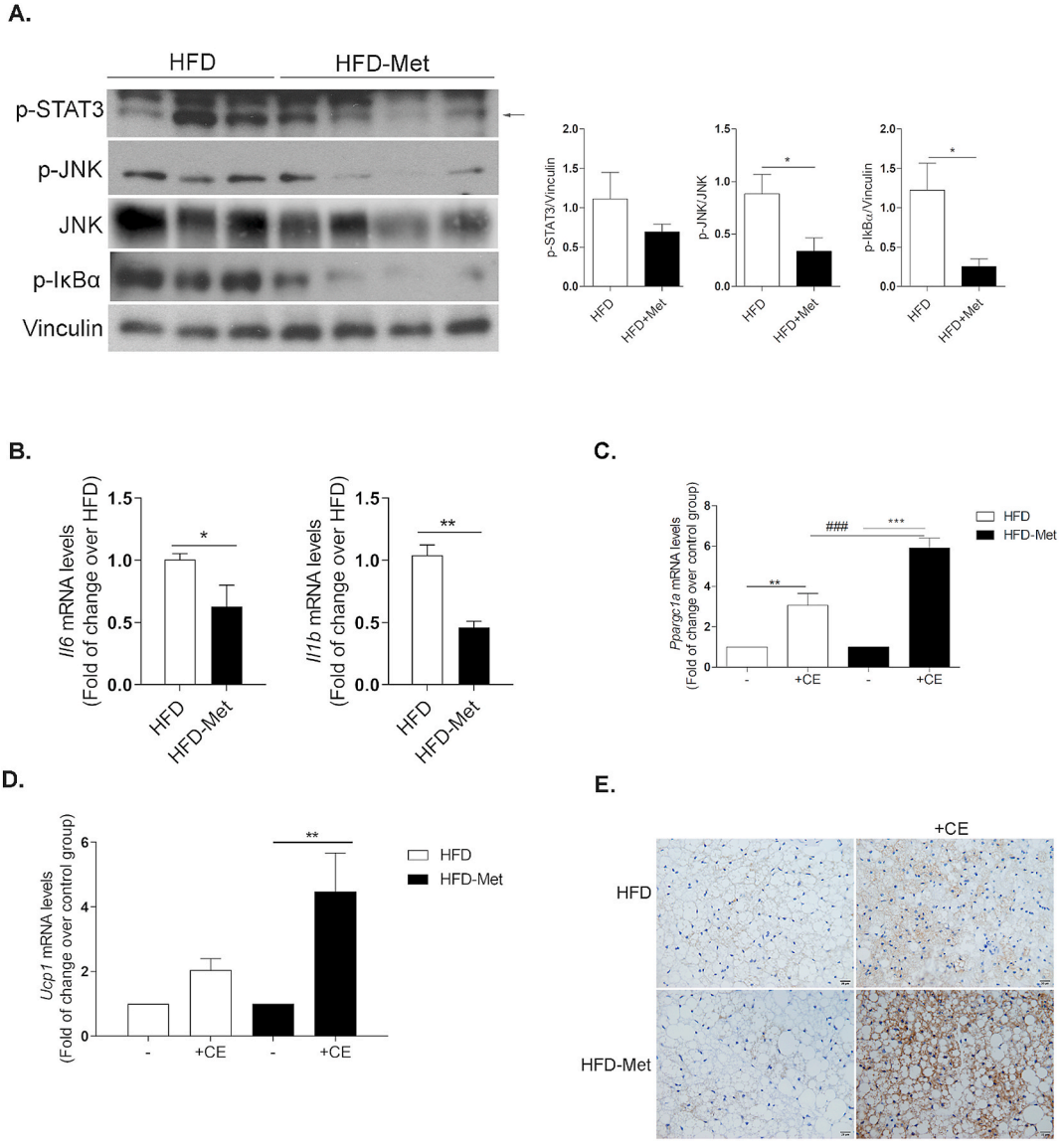

Fig. 4. *Treatment of obese mice with metformin reduced BAT inflammation and increased cold responsiveness.* **A)** Representative Western blot analysis of phosho-STAT3, phospho-JNK, JNK, phospho-IκBα and Vinculin in BAT from mice fed a HFD without (HFD) or with metformin treatment (HFD-Met) (n = 4 mice/group). *p < 0.05 versus HFD. **B)** mRNA levels of *Il6* and *Il1b* in BAT of HFD and HFD-Met groups (n = 4 mice/group). *p < 0.05, **p < 0.01 versus HFD. **C, D)** mRNA levels of *Ppargc1a and Ucp1* in BAT from HFD and HFD-Met mice exposed or not to 4 °C (CE) for 6 h (n = 4 mice/group). **p < 0.01, ***p < 0.001 versus non-cold exposure; $^{###}$p < 0.001 versus HFD cold exposure (CE). **E)** Representative images of UCP1 immunohistochemistry in BAT from HFD and HFD-Met mice exposed or not to 4 °C for 6 h (n = 4 mice/group). Data are shown as mean ± SEM. Statistical analysis was performed using two-tailed unpaired *t*-test when comparing two groups and one-way ANOVA followed by Tukey's post hoc test for multiple comparisons.

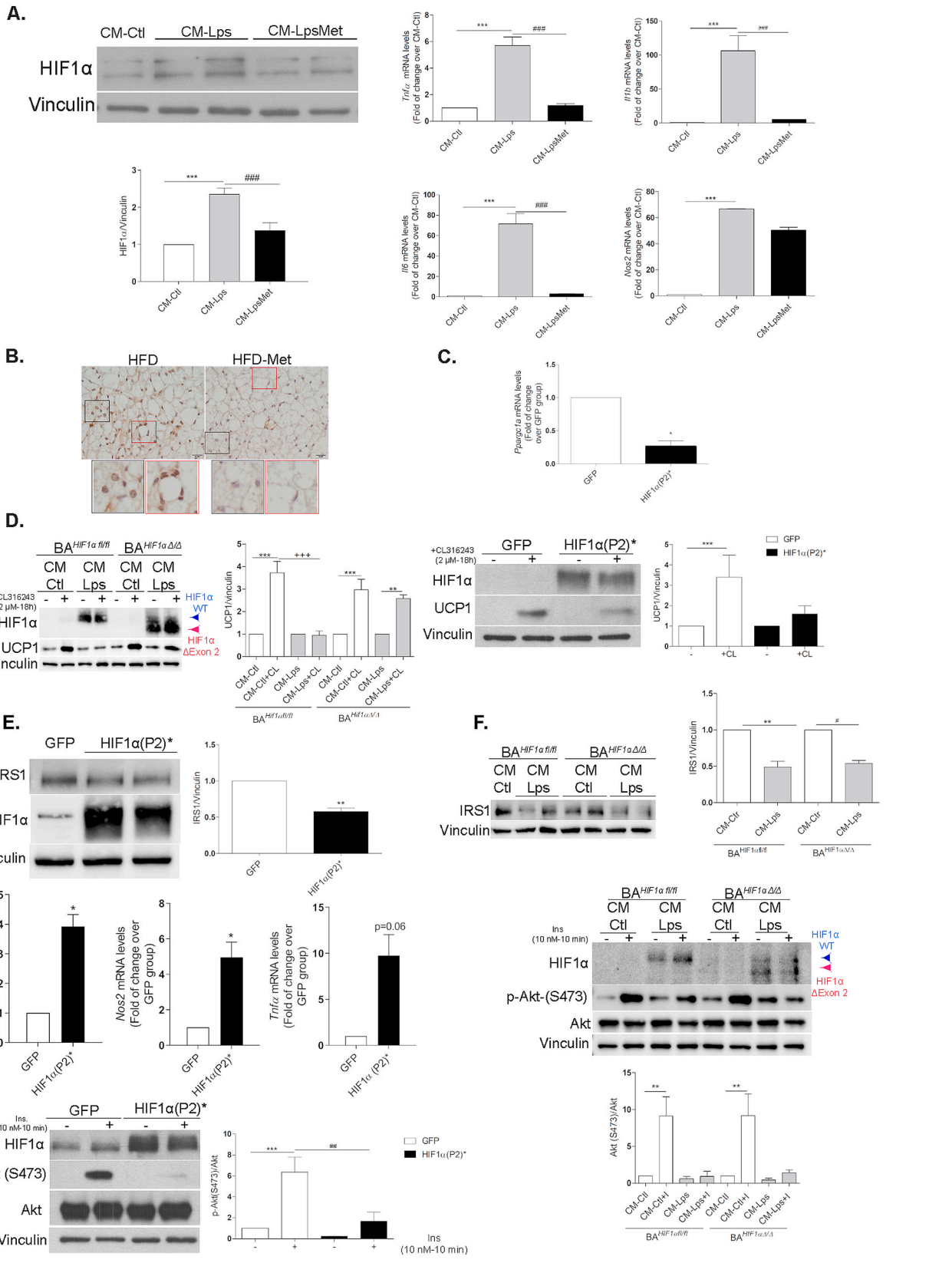

(caption on next page)

Fig. 5. Stabilization of HIF1α was sufficient to decrease insulin and β3-adrenergic responses in brown adipocytes. **A)** *(left panel)* Representative Western blots of HIF1α and Vinculin levels and quantification in differentiated brown adipocytes treated with CM-Ctl, CM-Lps and CM-LpsMet for 18 h (n = 3 independent experiments). (*right panel*) mRNA levels of *Tnfa*, *Il6*, *Il1b* and *Nos2* under similar experimental conditions (n = 3 independent experiments). ***p < 0.001 versus CM-Ctl; $^{###}$p < 0.001 versus CM-Lps. **B)** Representative images of HIF1α immunohistochemistry in BAT from HFD and HFD-Met mice (n = 4 mice/group). Black square: amplification image showing brown adipocyte nuclei. Red square: amplification image showing immune cell nuclei. **C)** mRNA levels of *Ppargc1a (upper panel)* and representative Western blot analysis of HIF1α, UCP1 and Vinculin levels and quantification (*lower panel*) in differentiated brown adipocytes expressing HIF1α(P2)* or GFP upon treatment or not with 2 μM CL316243 for 18 h (n = 3 independent experiments). *p < 0.05, ***p < 0.001 versus GFP **D)** BA$^{Hif1afl/fl}$ and BA$^{Hif1a\Delta/\Delta}$ were treated with CM-Ctl and CM-Lps for 18 h in the absence or presence of 2 μM CL316243 and the expression of HIF1α, UCP1, and Vinculin was analyzed by Western blot (n = 5 independent experiments). **p < 0.01, ***p < 0.001 versus without CL316243; $^{+++}$p<0.001 versus CM-Ctl + CL316243. **E)** (*upper panel*) Representative Western blot and quantification of HIF1α, IRS1 and Vinculin levels in differentiated brown adipocytes expressing HIF1α(P2)* and their corresponding GFP controls (n = 3 independent experiments). (*middle panel*) mRNA levels of *Il6*, *Tnfa* and *Nos2* (n = 3 independent experiments). *p < 0.05, **p < 0.01 versus GFP. (*lower panel*) Representative Western blot of HIF1α, phospho-Akt (Ser473), Akt and Vinculin levels and quantification in brown adipocytes overexpressing HIF1α(P2)* and GFP control cells upon stimulation with 10 nM insulin for 10 min (n = 4 independent experiments). ***p < 0.001 versus without insulin; $^{##}$p < 0.01 versus GFP + Insulin. **F)** (*upper panel*) Representative Western blot analysis of IRS1 and Vinculin protein levels and quantification in BA$^{Hif1afl/fl}$ and BA$^{Hif1a\Delta/\Delta}$ treated with CM-Ctl and CM-Lps for 24 h *p < 0.05, **p < 0.01 versus CM-Ctl. (*lower panel*) Representative Western blot of phosho-Akt (Ser473), Akt and Vinculin levels and quantification in BA$^{Hif1afl/fl}$ and BA$^{Hif1a\Delta/\Delta}$ cells treated with CM-Ctl and CM-Lps for 18 h followed by stimulation with 10 nM insulin for 10 min (n = 5 independent experiments). **p < 0.01 versus without insulin. Data are shown as mean ± SEM. Statistical analysis was performed using two-tailed unpaired *t*-test when comparing two groups and one-way ANOVA followed by Tukey's post hoc test for multiple comparisons. (For interpretation of the references to colour in this figure legend, the reader is referred to the Web version of this article.)

mutant resistant to degradation by PHDs [39,53]. Of note, HIF1α overexpression reached levels comparable to those of brown adipocytes treated with CM-Lps (Fig. S3). We first tested the response of brown adipocytes to CL316243. As shown in Fig. 5C, CL316243-mediated induction of *Ppargc1a* mRNA and UCP1 protein expression were reduced in brown adipocytes upon ectopic expression of HIF1α. Since these results indicated that stabilization of HIF1α is sufficient to impair thermogenic-related expression in brown adipocytes, we next evaluated whether endogenous HIF1α stabilization by CM-Lps-mediated inflammation is also responsible for the decline of UCP1. Fig. 5D shows that control brown adipocytes (BA$^{Hif1afl/fl}$) did not respond to CL316243 in the presence of CM-Lps while HIF1α-deficient brown adipocytes (BA$^{Hif1a\Delta/\Delta}$) retained CL316243-dependent UCP1 expression. These results suggest that HIF1α expressed in brown adipocytes is critical for the impairment of β-adrenergic-dependent UCP1 expression in an inflammatory context.

Proinflammatory environment leads to HIF1α-dependent and -independent suppression of insulin signaling in brown adipocytes. We next addressed the relevance of HIF1α in the impairment of insulin signaling under proinflammatory conditions. Ectopic expression of HIF1α in brown adipocytes markedly reduced IRS1 protein levels, as well as insulin-mediated Akt phosphorylation (Fig. 5E). Of note, *Il6, Tnfa and Nos2* mRNAs were elevated in HIF1α-transduced brown adipocytes (Fig. 5E), as occurred upon exposure to CM-Lps (Fig. 5A), suggesting that macrophage-dependent inflammatory signals activate a secondary inflammatory response in nearby brown adipocytes characterized by HIF1α-dependent *Il6*, *Tnfa,* and *Nos2* expression. Since it has been reported IRS1 serine 307 phosphorylation-mediated IRS1 degradation by inflammatory cytokines [48] and, therefore, not involving transcriptional mechanisms, we wanted to explore whether HIF1α stabilization is still relevant to reduce IRS1 levels in the presence of CM-Lps. As shown in Fig. 5F, IRS1 degradation and impaired insulin-induced Akt phosphorylation were also found in HIF1α-deficient brown adipocytes (BA$^{Hif1a\Delta/\Delta}$) exposed to CM-Lps. In fact, these cells lacking full-length HIF1α still showed marked activation of proinflammatory signaling and phosphorylation of IRS1 at serine 307 in the presence of CM-Lps (Fig. S4). These data led us to suggest that although HIF1α stabilization *per se* is sufficient to impair insulin signaling, the proinflammatory cytokine-enriched CM overrides HIF1α due to the ability to trigger IRS1 serine 307 phosphorylation, IRS1 degradation and an impairment of insulin signaling. In fact, direct addition of a cocktail of TNFα, IL6 and IL1β to brown adipocytes led to IRS1 degradation, resulting in impaired insulin-mediated Akt phosphorylation (Fig. S5).

The protective effect of metformin in the crosstalk between macrophages and brown adipocytes does not require AMPKα1. Interestingly, short-term stimulation of brown adipocytes with CM-LpsMet transiently increased AMPK phosphorylation (Fig. S6A). Notably, CM-LpsMet does not contain metformin since the drug was washed out as detailed in Materials and Methods. Moreover, as shown in Fig. S6B, the effect of CM-LpsMet in inducing AMPK phosphorylation in brown adipocytes was comparable to the response of brown adipocytes treated with CM-Ctl supplemented with metformin. To directly address if AMPK was required for the effect of CM-LpsMet in the protection of brown adipocytes against an inflammatory environment, we immortalized and differentiated brown adipocytes from AMPKα1-deficient mice (referred as BA$^{Ampka1-/-}$) (Fig. S6C) that, as shown in Fig. S6D, preserved the capacity to fully differentiate, as well as maintained insulin and CL316243 sensitivity in the presence of CM-LpsMet (Figs. S6E and S6F). These results suggest that in brown adipocytes AMPKα1 is dispensable to preserve the hormonal responses in the presence of proinflammatory CM-LpsMet.

Metformin alleviated BAT inflammation by promoting HIF1α degradation in macrophages. Since on the one hand, the secretome of macrophages receiving LPS and metformin protected brown adipocytes against inflammation and, on the other, treatment of HFD-fed mice with metformin reduced HIF1α levels in BAT, we postulated that metformin could modulate HIF1α in BAT macrophages and therefore, alleviate inflammation. In fact, Fig. 5B showed HIF1α immunostaining in immune cells in BAT. We also performed double HIF1α and F4/80 (as a marker of BAT macrophages) immunofluorescence in BAT sections. As shown in Fig. S7, HIF1α and F4/80 co-localized in areas of macrophages infiltration in BAT from obese mice similar to what was found in WAT [54], and this effect was ameliorated by the treatment with metformin. These results correlated with the absence of HIF1α and iNOS protein levels in macrophages treated with LPS and metformin (Fig. 6A). Moreover, the effects of LPS and metformin in HIF1α and iNOS expression were similar in BMDM from mice lacking AMPKα1 (Fig. S6G). On the contrary, the effect of metformin in preventing LPS-mediated HIF1α stabilization in macrophages was abolished in the presence of the proteasome inhibitor MG132, suggesting that metformin promotes HIF1α degradation via proteasome (Fig. 6A).

Then, we considered whether inhibition of mitochondrial complex I and oxygen consumption by metformin might redistribute the spared oxygen to reactivate PHDs leading to HIF1α degradation through the proteasome pathway. To further evaluate this possibility, we measured the activity of mitochondrial complex I and oxygen consumption rate (OCR) in Raw 267.4 macrophages. As shown in Fig. 6B, both parameters did not decrease significantly by LPS compared with the control cells, but were abrogated when metformin was added on LPS-treated cells. Similar modulation of the basal OCR by LPS and metformin in Raw 267.4 macrophages was observed in the Seahorse profile (Fig. 6C). In addition, mitochondrial mass and ROS production were analyzed by flow cytometry using Mitotracker Green and MitoSOX, respectively. The results revealed no significant differences among Raw 264.7

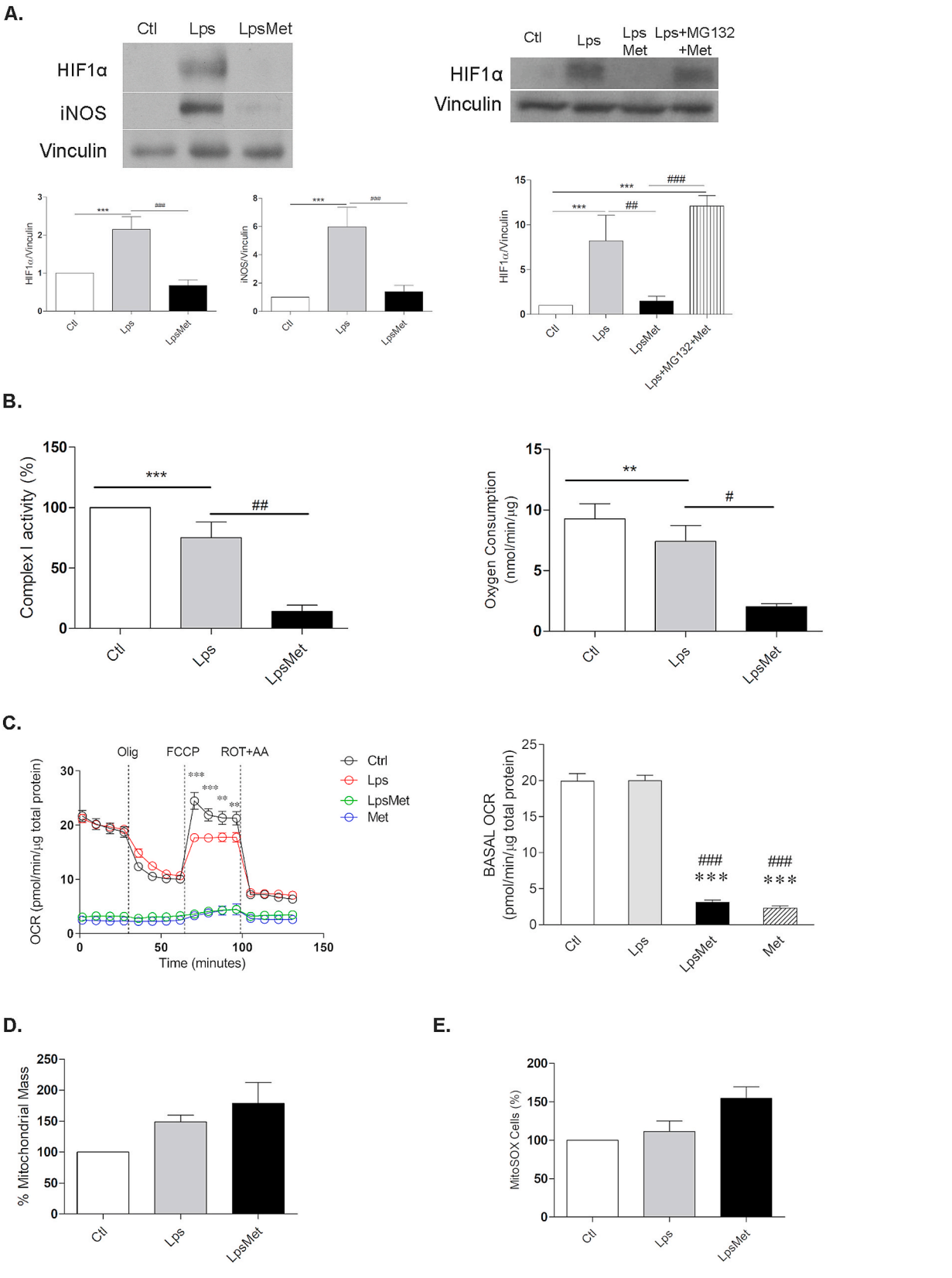

(caption on next page)

Fig. 6. *Metformin alleviated inflammation in macrophages independently of AMPKα1.* **A).** (*Left panel*) Representative Western blots of HIF1α, iNOS and Vinculin levels in BMDM from AMPKα1-deficient mice treated with LPS (Lps) or LPS and Metformin (LpsMet) as indicated in material and methods (n = 3 independent experiments). ***p < 0.001 versus Ctl; $^{###}$p < 0.001 versus Lps. (*Right panel*) Representative Western blots of HIF1α and Vinculin levels in Raw 246.7 macrophages treated as indicated in materials and methods. Proteasome activity was inhibited by addition of 1 μM MG-132 for 4 h before cell lysis. ***p < 0.001 versus Ctl; $^{++}$p<0.01 versus Lps; $^{###}$p < 0.001 versus LpsMet. **B)** (*Left panel*) Changes in mitochondrial complex I activity and (*Right panel*) oxygen consumption in Raw 264.7 macrophages in response to Lps or Lps and Metformin (LpsMet) treatment (n = 3 independent experiments). ***p < 0.001 versus Ctl, **p < 0.01 versus Ctl, $^{##}$p < 0.01 versus Lps, $^{#}$p < 0.05 versus Lps. **C)** (*Left panel*) Real-time changes in OCR of Raw 246.7 macrophages treated with Lps, Lps and Metformin or Metformin alone before treatment with oligomycin (Olig) (0.5 μM), FCCP (1 μM), and rotenone and antimycin A (ROT + AA) (0.5 μM). (*Right panel*) Basal respiratory capacity of Raw 246.7 macrophages treated with Lps, Lps and Metformin or Metformin alone (indicated in Material and Methods) before the starting Seahorse determinations. Average and standard deviation of 8 individual wells from two experiments is shown. Results are expressed as pmol/min/μg total protein. **p < 0.01 and ***p < 0.001 by two-way ANOVA compared with Ctl or $^{###}$p < 0.001 compared with Lps. **D)** Mitochondrial mass and **E)** MitoSOX positive cells analysis in Raw 246.7 macrophages treated with Lps or Lps and Metformin (LpsMet) (n = 4 independent experiments). Data are shown as mean ± SEM. Statistical analysis was performed using two-tailed unpaired *t*-test when comparing two groups and one-way ANOVA followed by Tukey's post hoc test for multiple comparisons.

macrophages untreated or treated with LPS in absence or presence of metformin (Fig. 6D and E). Therefore, it might be suggested that exposure to metformin by inhibiting mitochondrial complex I leads to increased oxygen availability (not consumed by mitochondria) for the prolyl-4-hydroxylase domain (PHD) oxygen sensors, which leads to enhanced HIF1α degradation. To reinforce this hypothesis, Raw 264.7 macrophages were treated with LPS in the absence or presence of the well-recognized complex I inhibitor rotenone. As shown in Figs. S8A and S8B, the combination of LPS and rotenone produced a similar effect in oxygen consumption and over HIF1α protein levels than that induced by LPS plus metformin (Fig. 6A and B), supporting the limitation of oxygen consumption by metformin as a trigger for HIF1α degradation in macrophages. A step further and in agreement with the results with metformin, when brown adipocytes were treated with the CM collected from Raw 264.7 macrophages stimulated with LPS plus rotenone (CM-LpsRtn), IRS1 levels were preserved as well as the response to insulin and CL316243 (Figs. S8C and S8D).

Inhibition of HIF1α in macrophages reduced the proinflammatory potency of CM-Lps and protected against insulin resistance in brown adipocytes. Since we found that the negative impact of HIF1α on insulin signaling in brown adipocytes is overridden by proinflammatory cytokines (Fig. S4), we tested whether HIF1α inhibition in macrophages might have a more profound effect. For this goal, Raw 264.7 macrophages were exposed to LPS together with a HIF1α inhibitor which represses its transcriptional activity [55,56]. Fig. 7A shows that co-treatment of macrophages with LPS and the HIF1α inhibitor blunted iNOS expression. We also determined the proinflammatory profile of the macrophages and found decreased *Il6* and *Il1b* mRNA levels in those co-treated with LPS and the HIF1α inhibitor (Fig. 7B) in parallel to a decrease in IL6 and IL1β content of the CM (referred as CM-InhLps) (Table S1).

Next, we analyzed the effect of HIF1α inhibition in macrophages in the crosstalk with brown adipocytes. Fig. 7C shows that STAT3, JNK and p38 MAPK phosphorylation in brown adipocytes stimulated with CM-Lps was attenuated when macrophages were treated with the HIF1α inhibitor. Consistently, the drop in insulin-induced Akt phosphorylation found in brown adipocytes exposed to CM-Lps was absent in the case of CM-InhLps (Fig. 7D). Also, brown adipocytes exposed to CM-InhLps were able to respond to CL316243 regarding UCP1 expression (Fig. 7E). Altogether, these results point to the relevance of HIF1α in the proinflammatory fate of macrophages leading to a secondary HIF1α activation in brown adipocytes that negatively modulates insulin and β-adrenergic responses of brown adipocytes.

4. Discussion

The molecular and cellular mechanisms involved in BAT dysfunction in the context of obesity are not completely understood. In particular, the interplay between macrophages and brown adipocytes is largely unknown. Herein, we provide *in vitro* settings that recapitulate precisely *in vivo* BAT dysfunction regarding insulin and adrenergic responsiveness, as well as the therapeutic benefit of metformin. Specifically, our results *in vitro* support the *in vivo* findings in obese mice regarding i) stabilization of HIF1α in BAT macrophages and reduction by metformin. ii) activation of proinflammatory signaling cascades and elevation of *Il1b* and *Il6* mRNA levels in BAT; both effects being also attenuated by metformin. iii) restoration by metformin of BAT responsiveness to cold exposure. Overall, our study has revealed relevant molecular insights in the role of macrophages in BAT dysfunction in obesity using both *in vitro* and in *vivo* settings.

Although HIF1α stabilization is mainly dependent on oxygen concentration, other studies have reported an oxygen-independent regulation of HIF1α by hyperglycemia, oxidative stress and, importantly, inflammatory mediators [57–59]. Our results have confirmed this alternative HIF1α induction under normoxic conditions in brown adipocytes exposed to the secretome of M1-polarized macrophages (CM-Lps) concurrently with intracellular pathways (*i.e.* STAT3, JNK, p38 MAPK and NFκB) and gene expression (*Tnfa*, *Il6*, *Il1b* and *Nos2*) associated to proinflammatory responses. This suggests that, under normoxic conditions, but in the context of local inflammation due to macrophage activation, brown adipocytes respond with HIF1α stabilization and induction of proinflammatory genes as occurred in white adipocytes [2,4,30,31]. As an additional sign of HIF1α activation, we also found that brown adipocytes exposed to the proinflammatory CM-Lps increased the expression levels of GLUT1, a direct target of HIF1α, resulting in elevated basal (insulin-independent) glucose uptake. A step further, inflammation-mediated HIF1α induction in brown adipocytes was able to attenuate insulin responses such as Akt phosphorylation and, hence, GLUT4 translocation to the plasma membrane and insulin-dependent glucose uptake. Both GLUT1 and glucose uptake were found elevated in human adipose stromal cells exposed to a mixture of TNFα, IL6 and IL1β [60] or in human and 3T3L1 adipocytes exposed to hypoxia [61,62]. Moreover, previous *in vivo* studies reported decreased Akt phosphorylation and glucose intolerance by HIF1α overexpression in adipose tissue [30]. Similarly, other studies conducted in adipocyte-specific HIF1α-deficient mice or mice treated with a HIF1α inhibitor showed protection against HFD-induced insulin resistance [30,32,63–68].

Of relevance, in brown adipocytes, the proinflammatory CM-Lps led to an increase in IRS1 phosphorylation at the modulatory serine 307 and the subsequent downregulation of its protein content as occurred with other metabolic stressors [48,69]. Our results show for the first time the downregulation of IRS1 protein by the ectopic expression of HIF1α in brown adipocytes concurrently with an elevation in *Tnfa, Il6,* and *Nos2* expression. Therefore, in brown adipocytes HIF1α-mediated elevation of proinflammatory cytokines could act in an autocrine manner, which might explain the downregulation of IRS1 and the subsequent decrease in insulin signaling. In addition, our data suggest that the proinflammatory cytokines present in the CM-Lps also impair insulin signaling involving other pathways such as a the rapid IRS1 serine 307 phosphorylation that overrides the impact of the HIF1α transcription program on IRS1 stability. Indeed, the CM-Lps was still competent to reduce IRS1 protein levels in HIF1α-deficient brown adipocytes, and the solely deletion of HIF1α was not able to rescue brown adipocytes from

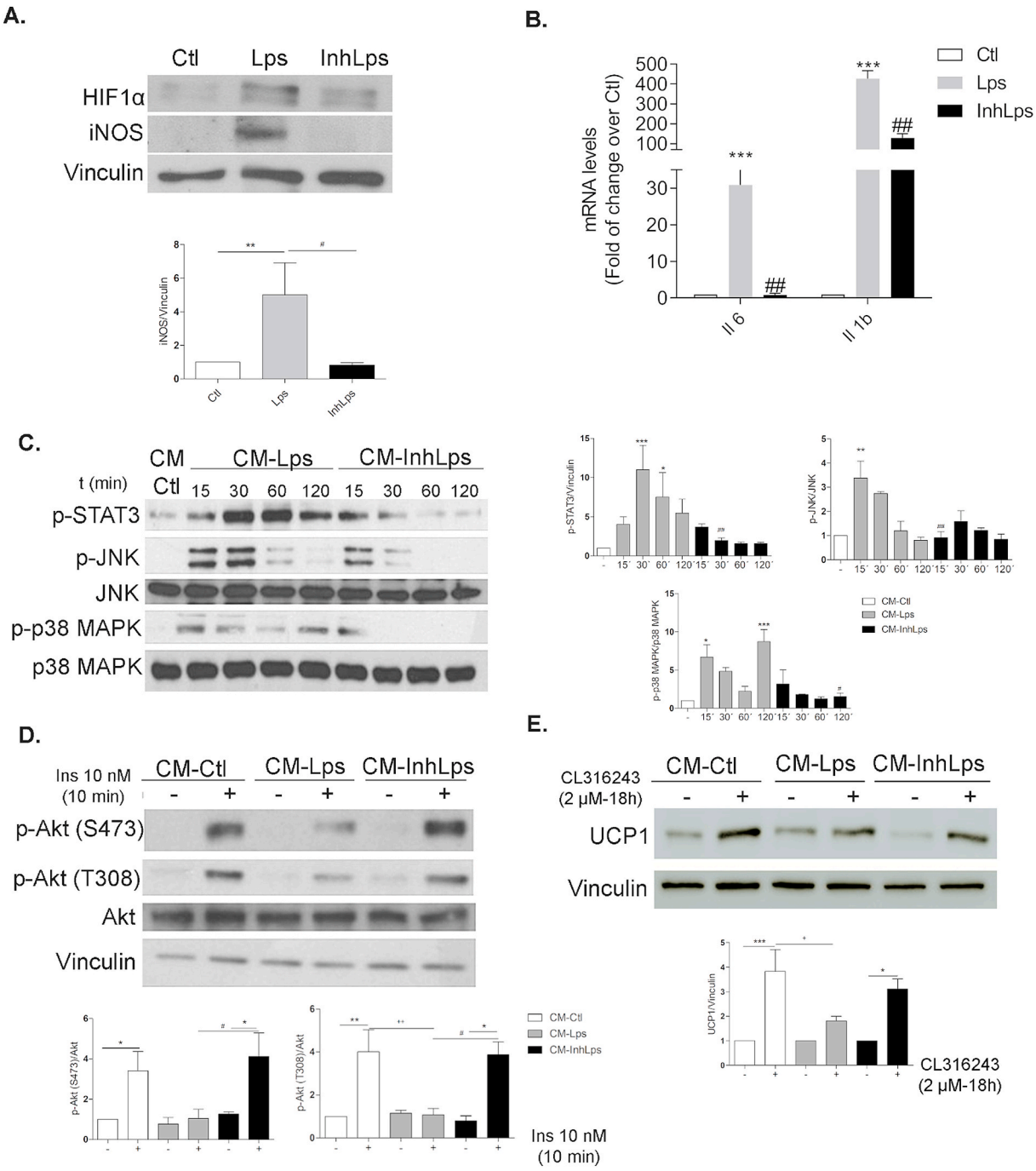

Fig. 7. Inhibition of HIF1α in macrophages reduced the proinflammatory potency of CM-Lps and protected against insulin resistance in brown adipocytes. **A)** Representative Western blots of HIF1α, iNOS and Vinculin levels in Raw 246.7 cells treated with LPS in the absence (Lps) or presence (InhLps) of a HIF1α inhibitor as indicated in material and methods (n = 3 independent experiments). $^{**}p < 0.01$ versus Ctl; $^{\#}p < 0.05$ versus Lps. **B)** mRNA levels of *Il6* and *Il1b* under similar experimental conditions (n = 3 independent experiments performed in duplicate). $^{***}p < 0.001$ versus Ctl; $^{\#\#}p < 0.01$ versus Lps. **C)** Representative Western blots of phospho-STAT3, phospho-JNK, JNK, phospho-p38 MAPK and p38 MAPK and quantification in brown adipocytes treated with CM-Ctl, CM-Lps or CM-InhLps for several time-periods (n = 3 independent experiments). $^{***}p < 0.001$, $^{**}p < 0.01$, $^{*}p < 0.05$ versus CM-Ctl; $^{\#}p < 0.05$, $^{\#\#}p < 0.01$ versus CM-Lps. **D)** Representative Western blots of phospho-Akt (Ser473), phospho-Akt (Thr308), Akt and Vinculin levels and quantification in brown adipocytes treated with CM-Ctl, CM-Lps or CM-InhLps for 18 h followed by stimulation with 10 nM insulin for 10 min (n = 5 independent experiments). $^{**}p < 0.01$, $^{*}p < 0.05$ versus without insulin; $^{++}p<0.01$ versus CM-Ctl + Insulin; $^{\#}p < 0.05$ versus CM-Lps + Insulin. **E)** Representative Western blots of UCP1 and vinculin protein levels and quantification in brown adipocytes stimulated with 2 μM CL316243 in the presence of CM-Ctl, CM-Lps or CM-InhLps for 18 h (n = 4 independent experiments). $^{*}p < 0.05$, $^{***}p < 0.001$ versus without CL316243; $^{+}p<0.05$ versus CM-Ctl + CL316243. Data are shown as mean ± SEM. Statistical analysis was performed using one-way ANOVA followed by Tukey's post hoc test.

insulin resistance. These data were supported by the protection against both HIF1α stabilization and inflammation-mediated IRS1 phosphorylation at serine 307 found in brown adipocytes exposed to the CM from macrophages treated with LPS and metformin (CM-LpsMet) that efficiently protected against proinflammatory signaling-mediated IRS1 degradation and insulin resistance. Interestingly, HIF1α-mediated decrease in IRS1 contrasts with the role of HIF2α in the liver positively modulating IRS2 expression and improving insulin sensitivity [70]. Thus, it seems that the two HIF isoforms might have contrasting actions on insulin signaling in a tissue-specific manner. Of relevance, in contrast to the beneficial effects of HIF1α deficiency, adipocyte-specific deletion of HIF2α in mice on a HFD increased inflammation and exacerbated insulin resistance [32]. In this line, antagonistic physiological or pathological functions of HIF isoforms have been reported in other cell types, including macrophages in which HIF1α modulates iNOS whereas HIF2α regulates arginase-1, readouts of M1 and M2 polarization, respectively [71].

In addition, the proinflammatory conditions surrounding brown adipocytes impaired the early steps of β-adrenergic signaling (*i.e.* HSL phosphorylation) and the lipolytic response as visualized by the higher size of the lipid droplets in brown adipocytes receiving CM-Lps and CL316243 compared to the controls. As expected from the impaired β-adrenergic signaling, *Ppargc1a* mRNA and UCP1 protein levels were significantly reduced in agreement with data in C3H10T1/2 (10T1/2) mouse mesenchymal stem cells [72] and our recent study [36]. Of relevance, herein we show that, in brown adipocytes, ectopic expression of HIF1α is sufficient to suppress their responses to CL316243. As such, either $BA^{Hif1a\Delta/\Delta}$ exposed to CM-Lps or wild-type brown adipocytes exposed to CM-LpsMet, which markedly reduced HIF1α levels, maintained β-adrenergic responsiveness, suggesting that stabilization of HIF1α is necessary and sufficient for attenuating the thermogenic responses of brown adipocytes in the context of inflammation. In this regard, our *in vitro* results could explain the reduced thermogenic function of BAT found in mice overexpressing HIF1α in adipose tissue [64].

An unresolved issue is whether inflammation in adipose tissue is an early trigger for HIF1α stabilization and if the subsequent HIF1α-mediated (hypoxia-related) gene response worsens the metabolic dysfunction in this tissue during obesity. In this line, our data show that the proinflammatory mediator LPS has the potential to induce primarily HIF1α in activated macrophages, which release cytokines that subsequently induce HIF1α in brown adipocytes under normoxic conditions. These data point out to the role of inflammation – and not necessarily hypoxia – in the activation of HIF1α in BAT tissue of obese mice. Accordingly, in BAT sections from HFD-fed mice we observed HIF1α immunostaining in macrophages that was nearly absent in mice treated with metformin, concomitantly with attenuated proinflammatory signaling cascades in this fat depot. Thus, our results revealed for the first time that, in addition to the role of HIF1α in brown adipocytes, stabilization of HIF1α in tissue macrophages is a key feature of BAT inflammation in obesity. In this regard, the expression of HIF1α in myeloid cells promotes inflammatory responses in WAT and tissue remodeling towards insulin resistance [73,74]. Also, Li and co-workers [73] associated the antiinflammatory effect of metformin with a reduction of HIF1α levels in WAT, thereby preventing inflammation and local fibrosis. These data prompted us to analyze the impact of metformin in the HIF1α-dependent proinflammatory profile of macrophages. We found that both the HIF1α inhibitor and metformin attenuated the proinflammatory responses in M1-(LPS-polarized) macrophages, as reported in other studies [33,46,47]. Moreover, our results showed that metformin promotes HIF1α degradation in macrophages via proteasome due to its well-known effect in reducing mitochondrial oxygen consumption by inhibiting mitochondrial complex I [5,75] without affecting mitochondrial ROS generation. Our data are in line with the study of Li et al. [73] showing an effect of metformin in 3T3L1 adipocytes by limiting oxygen consumption, thereby preventing hypoxia. This effect was further evaluated using rotenone, a well-known specific inhibitor of mitochondrial complex I and oxygen consumption. Indeed, rotenone, at doses that abrogated oxygen consumption, markedly reduced HIF1α accumulation in LPS-treated Raw 264.7 macrophages. Therefore, these results strongly suggest that metformin and rotenone decrease HIF1α by reducing mitochondrial oxygen consumption. Moreover, addition of rotenone as well as metformin to M1 polarized macrophages generated CM that prevented the attenuation of insulin and β-adrenergic responses in brown adipocytes. It is also important to highlight that the effect of metformin through inhibition of complex 1 is controversial [76] and, in this regard, the inhibition of hepatic gluconeogenesis by this drug independently of complex 1 activity has been reported [77].

Inflammation in BAT leads to the impairment of insulin and β-adrenergic responses *in vivo*, as we and others reported in *db/db* mice and mice injected LPS [30,36,55]. Regarding the impact of metformin in the interactome between macrophages and brown adipocytes in BAT functionality in obesity, we found an increase in *Ppargc1a* and *Ucp1* mRNAs, as well as UCP1 protein expression upon cold exposure in mice treated with metformin for 6 weeks, an effect likely related to the inhibition of HIF1α. A recent study associated the effect of metformin in HFD-fed mice with lipid metabolism in BAT by reducing *Cpt1b* and *Cpt2* expression [78]. These authors conclude that this reduction might attenuate diet-induced thermogenesis; although, this contrasts with the well-known relevance of fatty acid oxidation for BAT thermogenesis. Since our results evidence an increase in UCP1 upon cold exposure in BAT from HFD-fed mice receiving metformin and also an effect of this drug in attenuating HIF1α immunostaining in macrophages as discussed above, we suggest an additional effect of metformin in BAT metainflammation by targeting HIF1α in resident macrophages. Indeed, treatment of M1-polarized macrophages with either metformin or a HIF1α inhibitor led to the production of CM that did not increase HIF1α (in the case of CM-LpsMet) or triggered proinflammatory signaling cascades when added to brown adipocytes, thereby favoring insulin and β-adrenergic responsiveness. For metformin, this effect concurred with a reduction of HIF1α in both macrophages and brown adipocytes, independently of AMPKα1. However, we cannot exclude a role for AMPKα2 in the effects of CM-LpsMet in brown adipocytes since this subunit is also expressed in BAT [79]. In addition to the mechanistic insights provided herein in cell-based systems, additional *in vivo* research will be needed to prove that metformin directly acts on BAT macrophages.

Evidence reported so far that metformin may influence tumor progression by modulating the responses of the tumor microenvironment, including reduction of tumor-associated macrophages [80,81]. Nevertheless, to the best of our knowledge, this is the first study reporting the protective effect of this antidiabetic drug in brown adipocytes specifically by targeting macrophages and reducing HIF1α-dependent brown adipocyte dysfunction. These results might have therapeutic relevance to alleviate BAT metainflammation in obesity.

Authors contribution

Conceptualization, A.M.V., N.P.; Funding Acquisition, A.M.V., M.J. O., M.AF-M., J.A. B.V., Investigation, N.P. V.F, P.V., E.M.E., C.E-G., M.P. V., L.R., C.G-P., I.G.M., A.A.U. Supervision, A.M.V., N.P.; Writing Original Draft, Review, and Editing, A.M.V., N.P., J.A. All Authors revised and approved the final version of the manuscript.

Declaration of competing interest

The authors declare no competing interests.

Acknowledgements

This work was funded by grants RTI2018-094052-B-100 (MCIN/AEI/10.13039/501100011033/FEDER) , S2017/BMD-3684 (Comunidad de Madrid, Spain), Fundación Ramón Areces (Spain) and CIBERdem (ISCIII) to A.M.V., grant S2010/BMD-2423 (Comunidad de Madrid,

Spain) to M.J.O. and A.M.V., PID2019-106371RB-I00 (MCIN/ AEI /10.13039/501100011033/ FEDER) to J.A and PI16/00789 (ISCIII, Spain) to M.A.F.-M. We also acknowledge all members of AMV's laboratory for helpful discussions. M.F. and B.V were supported by Inserm, CNRS, Université de Paris, and Région Ile-de-France. We also acknowledge the EFSD Albert Reynolds travel grant fellowship to V.F.

Appendix A. Supplementary data

Supplementary data to this article can be found online at https://doi.org/10.1016/j.redox.2021.102171.

References

[1] Y.C. Chooi, C. Ding, F. Magkos, The epidemiology of obesity, Metabolism 92 (2019) 6–10.
[2] L. Dowal, P. Parameswaran, S. Phat, S. Akella, I.D. Majumdar, J. Ranjan, C. Shah, S. Mogre, K. Guntur, K. Thapa, S. Gesta, V.K. Vishnudas, N.R. Narain, R. Sarangarajan, Intrinsic Properties of Brown and White Adipocytes Have Differential Effects on Macrophage Inflammatory Responses, Mediators Inflamm, 2017, 9067049, 2017.
[3] B.A. Swinburn, G. Sacks, K.D. Hall, K. Mcpherson, D.T. Finegood, M.L. Moodie, S. L. Gortmaker, The global obesity pandemic: shaped by global drivers and local environments, Lancet 378 (2011) 804–814.
[4] A.R. Saltiel, J.M. Olefsky, Inflammatory mechanisms linking obesity and metabolic disease, J. Clin. Invest. 127 (2017) 1–4.
[5] C. Batandier, B. Guigas, D. Detaille, M.Y. El-Mir, E. Fontaine, M. Rigoulet, X. M. Leverve, The ROS production induced by a reverse-electron flux at respiratory-chain complex 1 is hampered by metformin, J. Bioenerg. Biomembr. 38 (2006) 33–42.
[6] V. Albert, K. Svensson, M. Shimobayashi, M. Colombi, S. Munoz, V. Jimenez, C. Handschin, F. Bosch, M.N. Hall, mTORC2 sustains thermogenesis via Akt-induced glucose uptake and glycolysis in brown adipose tissue, EMBO Mol. Med. 8 (2016) 232–246.
[7] A.M. Cypess, S. Lehman, G. Williams, I. Tal, D. Rodman, A.B. Goldfine, F.C. Kuo, E. L. Palmer, Y.H. Tseng, A. Doria, G.M. Kolodny, C.R. Kahn, Identification and importance of brown adipose tissue in adult humans, N. Engl. J. Med. 360 (2009) 1509–1517.
[8] J. Nedergaard, T. Bengtsson, B. Cannon, Unexpected evidence for active brown adipose tissue in adult humans, Am. J. Physiol. Endocrinol. Metab. 293 (2007) E444–E452.
[9] C. Scheele, S. Nielsen, Metabolic regulation and the anti-obesity perspectives of human brown fat, Redox Biol 12 (2017) 770–775.
[10] B.P. Leitner, S. Huang, R.J. Brychta, C.J. Duckworth, A.S. Baskin, S. Mcgehee, I. Tal, W. Dieckmann, G. Gupta, G.M. Kolodny, K. Pacak, P. Herscovitch, A. M. Cypess, K.Y. Chen, Mapping of human brown adipose tissue in lean and obese young men, Proc. Natl. Acad. Sci. U. S. A. 114 (2017) 8649–8654.
[11] Q. Wang, M. Zhang, M. Xu, W. Gu, Y. Xi, L. Qi, B. Li, W. Wang, Brown adipose tissue activation is inversely related to central obesity and metabolic parameters in adult human, PLoS One 10 (2015), e0123795.
[12] M. Alcala, M. Calderon-Dominguez, E. Bustos, P. Ramos, N. Casals, D. Serra, M. Viana, L. Herrero, Increased inflammation, oxidative stress and mitochondrial respiration in brown adipose tissue from obese mice, Sci. Rep. 7 (2017) 16082.
[13] T. Sakamoto, T. Nitta, K. Maruno, Y.S. Yeh, H. Kuwata, K. Tomita, T. Goto, N. Takahashi, T. Kawada, Macrophage infiltration into obese adipose tissues suppresses the induction of UCP1 level in mice, Am. J. Physiol. Endocrinol. Metab. 310 (2016) E676–E687.
[14] P. Gonzalez-Muniesa, L. Garcia-Gerique, P. Quintero, S. Arriaza, A. Lopez-Pascual, J.A. Martinez, Effects of Hyperoxia on Oxygen-Related Inflammation with a Focus on Obesity. Oxid Med Cell Longev, 2015, p. 8957827, 2015.
[15] R. Norouzirad, P. Gonzalez-Muniesa, A. Ghasemi, Hypoxia in obesity and diabetes: potential therapeutic effects of hyperoxia and nitrate, Oxid Med Cell Longev (2017), 5350267, 2017.
[16] S.M. Reilly, A.R. Saltiel, Adapting to obesity with adipose tissue inflammation, Nat. Rev. Endocrinol. 13 (2017) 633–643.
[17] G.L. Semenza, Oxygen sensing, hypoxia-inducible factors, and disease pathophysiology, Annu. Rev. Pathol. 9 (2014) 47–71.
[18] P. Jaakkola, D.R. Mole, Y.M. Tian, M.I. Wilson, J. Gielbert, S.J. Gaskell, A. Von Kriegsheim, H.F. Hebestreit, M. Mukherji, C.J. Schofield, P.H. Maxwell, C.W. Pugh, P.J. Ratcliffe, Targeting of HIF-alpha to the von Hippel-Lindau ubiquitylation complex by O2-regulated prolyl hydroxylation, Science 292 (2001) 468–472.
[19] G.L. Semenza, Hypoxia-inducible factor 1 and cardiovascular disease, Annu. Rev. Physiol. 76 (2014) 39–56.
[20] E.L. Bell, T.A. Klimova, J. Eisenbart, C.T. Moraes, M.P. Murphy, G.R. Budinger, N. S. Chandel, The Qo site of the mitochondrial complex III is required for the transduction of hypoxic signaling via reactive oxygen species production, J. Cell Biol. 177 (2007) 1029–1036.
[21] J.K. Brunelle, E.L. Bell, N.M. Quesada, K. Vercauteren, V. Tiranti, M. Zeviani, R. C. Scarpulla, N.S. Chandel, Oxygen sensing requires mitochondrial ROS but not oxidative phosphorylation, Cell Metabol. 1 (2005) 409–414.
[22] N.S. Chandel, D.S. Mcclintock, C.E. Feliciano, T.M. Wood, J.A. Melendez, A. M. Rodriguez, P.T. Schumacker, Reactive oxygen species generated at mitochondrial complex III stabilize hypoxia-inducible factor-1alpha during hypoxia: a mechanism of O2 sensing, J. Biol. Chem. 275 (2000) 25130–25138.
[23] R.D. Guzy, B. Hoyos, E. Robin, H. Chen, L. Liu, K.D. Mansfield, M.C. Simon, U. Hammerling, P.T. Schumacker, Mitochondrial complex III is required for hypoxia-induced ROS production and cellular oxygen sensing, Cell Metabol. 1 (2005) 401–408.
[24] K.D. Mansfield, R.D. Guzy, Y. Pan, R.M. Young, T.P. Cash, P.T. Schumacker, M. C. Simon, Mitochondrial dysfunction resulting from loss of cytochrome c impairs cellular oxygen sensing and hypoxic HIF-alpha activation, Cell Metabol. 1 (2005) 393–399.
[25] D. Gerald, E. Berra, Y.M. Frapart, D.A. Chan, A.J. Giaccia, D. Mansuy, J. Pouyssegur, M. Yaniv, F. Mechta-Grigoriou, JunD reduces tumor angiogenesis by protecting cells from oxidative stress, Cell 118 (2004) 781–794.
[26] C. Schroedl, D.S. Mcclintock, G.R. Budinger, N.S. Chandel, Hypoxic but not anoxic stabilization of HIF-1alpha requires mitochondrial reactive oxygen species, Am. J. Physiol. Lung Cell Mol. Physiol. 283 (2002) L922–L931.
[27] C.C. Blouin, E.L. Page, G.M. Soucy, D.E. Richard, Hypoxic gene activation by lipopolysaccharide in macrophages: implication of hypoxia-inducible factor 1alpha, Blood 103 (2004) 1124–1130.
[28] K. Nishi, T. Oda, S. Takabuchi, S. Oda, K. Fukuda, T. Adachi, G.L. Semenza, K. Shingu, K. Hirota, LPS induces hypoxia-inducible factor 1 activation in macrophage-differentiated cells in a reactive oxygen species-dependent manner, Antioxidants Redox Signal. 10 (2008) 983–995.
[29] S. Frede, C. Stockmann, P. Freitag, J. Fandrey, Bacterial lipopolysaccharide induces HIF-1 activation in human monocytes via p44/42 MAPK and NF-kappaB, Biochem. J. 396 (2006) 517–527.
[30] N. Halberg, T. Khan, M.E. Trujillo, I. Wernstedt-Asterholm, A.D. Attie, S. Sherwani, Z.V. Wang, S. Landskroner-Eiger, S. Dineen, U.J. Magalang, R.A. Brekken, P. E. Scherer, Hypoxia-inducible factor 1alpha induces fibrosis and insulin resistance in white adipose tissue, Mol. Cell Biol. 29 (2009) 4467–4483.
[31] C. Jiang, A. Qu, T. Matsubara, T. Chanturiya, W. Jou, O. Gavrilova, Y.M. Shah, F. J. Gonzalez, Disruption of hypoxia-inducible factor 1 in adipocytes improves insulin sensitivity and decreases adiposity in high-fat diet-fed mice, Diabetes 60 (2011) 2484–2495.
[32] Y.S. Lee, J.W. Kim, O. Osborne, D.Y. Oh, R. Sasik, S. Schenk, A. Chen, H. Chung, A. Murphy, S.M. Watkins, O. Quehenberger, R.S. Johnson, J.M. Olefsky, Increased adipocyte O2 consumption triggers HIF-1alpha, causing inflammation and insulin resistance in obesity, Cell 157 (2014) 1339–1352.
[33] A.R. Cameron, V.L. Morrison, D. Levin, M. Mohan, C. Forteath, C. Beall, A. D. Mcneilly, D.J. Balfour, T. Savinko, A.K. Wong, B. Viollet, K. Sakamoto, S. C. Fagerholm, M. Foretz, C.C. Lang, G. Rena, Anti-inflammatory effects of metformin irrespective of diabetes status, Circ. Res. 119 (2016) 652–665.
[34] N. Gamad, S. Malik, K. Suchal, S. Vasisht, A. Tomar, S. Arava, D.S. Arya, J. Bhatia, Metformin alleviates bleomycin-induced pulmonary fibrosis in rats: pharmacological effects and molecular mechanisms, Biomed. Pharmacother. 97 (2018) 1544–1553.
[35] X. Luo, R. Hu, Y. Zheng, S. Liu, Z. Zhou, Metformin shows anti-inflammatory effects in murine macrophages through Dicer/microribonucleic acid-34a-5p and microribonucleic acid-125b-5p, J Diabetes Investig 11 (2020) 101–109.
[36] C. Escalona-Garrido, P. Vazquez, P. Mera, S. Zagmutt, E. Garcia-Casarrubios, A. Montero-Pedrazuela, F. Rey-Stolle, A. Guadano-Ferraz, F.J. Ruperez, D. Serra, L. Herrero, M.J. Obregon, A.M. Valverde, Moderate SIRT1 overexpression protects against brown adipose tissue inflammation, Mol Metab 42 (2020), 101097.
[37] S.B. Jorgensen, B. Viollet, F. Andreelli, C. Frosig, J.B. Birk, P. Schjerling, S. Vaulont, E.A. Richter, J.F. Wojtaszewski, Knockout of the alpha2 but not alpha1 5'-AMP-activated protein kinase isoform abolishes 5-aminoimidazole-4-carboxa-mide-1-beta-4-ribofuranosidebut not contraction-induced glucose uptake in skeletal muscle, J. Biol. Chem. 279 (2004) 1070–1079.
[38] H.E. Ryan, M. Poloni, W. Mcnulty, D. Elson, M. Gassmann, J.M. Arbeit, R. S. Johnson, Hypoxia-inducible factor-1alpha is a positive factor in solid tumor growth, Cancer Res. 60 (2000) 4010–4015.
[39] D. Labrousse-Arias, R. Castillo-Gonzalez, N.M. Rogers, M. Torres-Capelli, B. Barreira, J. Aragones, A. Cogolludo, J.S. Isenberg, M.J. Calzada, HIF-2alpha-mediated induction of pulmonary thrombospondin-1 contributes to hypoxia-driven vascular remodelling and vasoconstriction, Cardiovasc. Res. 109 (2016) 115–130.
[40] Q. Yan, S. Bartz, M. Mao, L. Li, W.G. Kaelin JR., The hypoxia-inducible factor 2alpha N-terminal and C-terminal transactivation domains cooperate to promote renal tumorigenesis in vivo, Mol. Cell Biol. 27 (2007) 2092–2102.
[41] Y.D. Liang, W.J. Bai, C.G. Li, L.H. Xu, H.X. Wei, H. Pan, X.H. He, D.Y. Ouyang, Piperine suppresses pyroptosis and interleukin-1beta release upon ATP triggering and bacterial infection, Front. Pharmacol. 7 (2016) 390.
[42] L.C. Green, D.A. Wagner, J. Glogowski, P.L. Skipper, J.S. Wishnok, S. R. Tannenbaum, Analysis of nitrate, nitrite, and [15N]nitrate in biological fluids, Anal. Biochem. 126 (1982) 131–138.
[43] A.M. Valverde, P. Navarro, M. Benito, M. Lorenzo, H-ras induces glucose uptake in brown adipocytes in an insulin- and phosphatidylinositol 3-kinase-independent manner, Exp. Cell Res. 243 (1998) 274–281.
[44] G. Hofhaus, R.M. Shakeley, G. Attardi, Use of polarography to detect respiration defects in cell cultures, Methods Enzymol. 264 (1996) 476–483.
[45] F. Medja, S. Allouche, P. Frachon, C. Jardel, M. Malgat, B. Mousson De Camaret, A. Slama, J. Lunardi, J.P. Mazat, A. Lombes, Development and implementation of standardized respiratory chain spectrophotometric assays for clinical diagnosis, Mitochondrion 9 (2009) 331–339.
[46] Y. Jing, F. Wu, D. Li, L. Yang, Q. Li, R. Li, Metformin improves obesity-associated inflammation by altering macrophages polarization, Mol. Cell. Endocrinol. 461 (2018) 256–264.

[47] J. Kim, H.J. Kwak, J.Y. Cha, Y.S. Jeong, S.D. Rhee, K.R. Kim, H.G. Cheon, Metformin suppresses lipopolysaccharide (LPS)-induced inflammatory response in murine macrophages via activating transcription factor-3 (ATF-3) induction, J. Biol. Chem. 289 (2014) 23246–23255.
[48] S. Bhattacharyya, L. Feferman, J.K. Tobacman, Carrageenan inhibits insulin signaling through GRB10-mediated decrease in Tyr(P)-IRS1 and through inflammation-induced increase in ser(P)307-IRS1, J. Biol. Chem. 290 (2015) 10764–10774.
[49] D.B. Savage, K.F. Petersen, G.I. Shulman, Mechanisms of insulin resistance in humans and possible links with inflammation, Hypertension 45 (2005) 828–833.
[50] V. Pardo, A. Gonzalez-Rodriguez, C. Guijas, J. Balsinde, A.M. Valverde, Opposite cross-talk by oleate and palmitate on insulin signaling in hepatocytes through macrophage activation, J. Biol. Chem. 290 (2015) 11663–11677.
[51] C. Peyssonnaux, P. Cejudo-Martin, A. Doedens, A.S. Zinkernagel, R.S. Johnson, V. Nizet, Cutting edge: essential role of hypoxia inducible factor-1alpha in development of lipopolysaccharide-induced sepsis, J. Immunol. 178 (2007) 7516–7519.
[52] G.M. Tannahill, A.M. Curtis, J. Adamik, E.M. Palsson-Mcdermott, A.F. Mcgettrick, G. Goel, C. Frezza, N.J. Bernard, B. Kelly, N.H. Foley, L. Zheng, A. Gardet, Z. Tong, S.S. Jany, S.C. Corr, M. Haneklaus, B.E. Caffrey, K. Pierce, S. Walmsley, F. C. Beasley, E. Cummins, V. NIizet, M. Whyte, C.T. Taylor, H. Lin, S.L. Masters, E. Gottlieb, V.P. Kelly, C. Clish, P.E. Auron, R.J. Xavier, L.A. O'NEeill, Succinate is an inflammatory signal that induces IL-1beta through HIF-1alpha, Nature 496 (2013) 238–242.
[53] F. Melendez-Rodriguez, A.A. Urrutia, D. Lorendeau, G. Rinaldi, O. Roche, N. Bogurcu-Seidel, M. Ortega Muelas, C. Mesa-Ciller, G. Turiel, A. Bouthelier, P. Hernansanz-Agustin, A. Elorza, E. Escasany, Q.O.Y. Li, M. Torres-Capelli, D. Tello, E. Fuertes, E. Fraga, A. Martinez-Ruiz, B. Perez, J.M. Gimenez-Bachs, A. S. Salinas-Sanchez, T. Acker, R. Sanchez Prieto, S.M. Fendt, K. De Bock, J. Aragones, HIF1alpha suppresses tumor cell proliferation through inhibition of Aspartate Biosynthesis, Cell Rep. 26 (2019) 2257–2265 e4.
[54] M. Sharma, L. Boytard, T. Hadi, G. Koelwyn, R. Simon, M. Ouimet, L. Seifert, W. Spiro, B. Yan, S. Hutchison, E.A. Fisher, R. Ramasamy, B. Ramkhelawon, K. J. Moore, Enhanced glycolysis and HIF-1alpha activation in adipose tissue macrophages sustains local and systemic interleukin-1beta production in obesity, Sci. Rep. 10 (2020) 5555.
[55] Y.F. Chen, S. Pandey, C.H. Day, Y.F. Chen, A.Z. Jiang, T.J. Ho, R.J. Chen, V. V. Padma, W.W. Kuo, C.Y. Huang, Synergistic effect of HIF-1alpha and FoxO3a trigger cardiomyocyte apoptosis under hyperglycemic ischemia condition, J. Cell. Physiol. 233 (2018) 3660–3671.
[56] R. Yamazaki, Y. Kasuya, T. Fujitha, H. Umezawa, M. Yanagihara, H. Nakamura, I. Yoshino, K. Tatsumi, T. Murayama, Antifibrotic effects of cyclosporine A on TGF-beta1-treated lung fibroblasts and lungs from bleomycin-treated mice: role of hypoxia-inducible factor-1alpha, Faseb. J. 31 (2017) 3359–3371.
[57] S.B. Catrina, Impaired hypoxia-inducible factor (HIF) regulation by hyperglycemia, J. Mol. Med. (Berl.) 92 (2014) 1025–1034.
[58] S.E. Corcoran, L.A. O'neill, HIF1alpha and metabolic reprogramming in inflammation, J. Clin. Invest. 126 (2016) 3699–3707.
[59] T. Cramer, Y. Yamanishi, B.E. Clausen, I. Forster, R. Pawlinski, N. Mackman, V. H. Haase, R. Jaenisch, M. Corr, V. Nizet, G.S. Firestein, H.P. Gerber, N. Ferrara, R. S. Johnson, HIF-1alpha is essential for myeloid cell-mediated inflammation, Cell 112 (2003) 645–657.
[60] M.M. Docanto, S. Ham, A. Corbould, K.A. Brown, Obesity-associated inflammatory cytokines and prostaglandin E2 stimulate glucose Transporter mRNA expression and glucose uptake in primary human adipose stromal cells, J. Interferon Cytokine Res. 35 (2015) 600–605.
[61] I.S. Wood, B. Wang, S. Lorente-Cebrian, P. Trayhurn, Hypoxia increases expression of selective facilitative glucose transporters (GLUT) and 2-deoxy-D-glucose uptake in human adipocytes, Biochem. Biophys. Res. Commun. 361 (2007) 468–473.
[62] J. Yin, Z. Gao, D. Liu, Z. Liu, J. Ye, Berberine improves glucose metabolism through induction of glycolysis, Am. J. Physiol. Endocrinol. Metab. 294 (2008) E148–E156.
[63] C. Jiang, J.H. Kim, F. Li, A. Qu, O. Gavrilova, Y.M. Shah, F.J. Gonzalez, Hypoxia-inducible factor 1alpha regulates a SOCS3-STAT3-adiponectin signal transduction pathway in adipocytes, J. Biol. Chem. 288 (2013) 3844–3857.
[64] J.C. Jun, R. Devera, D. Unnikrishnan, M.K. Shin, S. Bevans-Fonti, Q. Yao, A. Rathore, H. Younas, N. Halberg, P.E. Scherer, V.Y. Polotsky, Adipose HIF-1alpha causes obesity by suppressing brown adipose tissue thermogenesis, J. Mol. Med. (Berl.) 95 (2017) 287–297.
[65] Y. Kihira, M. Miyake, M. Hirata, Y. Hoshina, K. Kato, H. Shirakawa, H. Sakaue, N. Yamano, Y. Izawa-Ishizawa, K. Ishizawa, Y. Ikeda, K. Tsuchiya, T. Tamaki, S. Tomita, Deletion of hypoxia-inducible factor-1alpha in adipocytes enhances glucagon-like peptide-1 secretion and reduces adipose tissue inflammation, PLoS One 9 (2014), e93856.
[66] J. Krishnan, C. Danzer, T. Simka, J. Ukropec, K.M. Walter, S. Kumpf, P. Mirtschink, B. Ukropcova, D. Gasperikova, T. Pedrazzini, W. Krek, Dietary obesity-associated Hif1alpha activation in adipocytes restricts fatty acid oxidation and energy expenditure via suppression of the Sirt2-NAD+ system, Genes Dev. 26 (2012) 259–270.
[67] C. Regazzetti, P. Peraldi, T. Gremeaux, R. Najem-Lendom, I. Ben-Sahra, M. Cormont, F. Bost, Y. Le Marchand-Brustel, J.F. Tanti, S. Giorgetti-Peraldi, Hypoxia decreases insulin signaling pathways in adipocytes, Diabetes 58 (2009) 95–103.
[68] K. Sun, N. Halberg, M. Khan, U.J. Magalang, P.E. Scherer, Selective inhibition of hypoxia-inducible factor 1alpha ameliorates adipose tissue dysfunction, Mol. Cell Biol. 33 (2013) 904–917.
[69] N.J. Hancer, W. Qiu, C. Cherella, Y. Li, K.D. Copps, M.F. White, Insulin and metabolic stress stimulate multisite serine/threonine phosphorylation of insulin receptor substrate 1 and inhibit tyrosine phosphorylation, J. Biol. Chem. 289 (2014) 12467–12484.
[70] C.M. Taniguchi, E.C. Finger, A.J. Krieg, C. Wu, A.N. Diep, E.L. Lagory, K. Wei, L. M. Mcginnis, J. Yuan, C.J. Kuo, A.J. Giaccia, Cross-talk between hypoxia and insulin signaling through Phd3 regulates hepatic glucose and lipid metabolism and ameliorates diabetes, Nat. Med. 19 (2013) 1325–1330.
[71] N. Takeda, E.L. O'Dea, A. Doedens, J.W. Kim, A. Weidemann, C. Stockmann, M. Asagiri, M.C. Simon, A. Hoffmann, R.S. Johnson, Differential activation and antagonistic function of HIF-{alpha} isoforms in macrophages are essential for NO homeostasis, Genes Dev. 24 (2010) 491–501.
[72] T. Goto, S. Naknukool, R. Yoshitake, Y. Hanafusa, S. Tokiwa, Y. Li, T. Sakamoto, T. Nitta, M. Kim, N. Takahashi, R. Yu, H. Daiyasu, S. Seno, H. Matsuda, T. Kawada, Proinflammatory cytokine interleukin-1beta suppresses cold-induced thermogenesis in adipocytes, Cytokine 77 (2016) 107–114.
[73] X. Li, J. Li, L. Wang, A. Li, Z. Qiu, L.W. Qi, J. Kou, K. Liu, B. Liu, F. Huang, The role of metformin and resveratrol in the prevention of hypoxia-inducible factor 1alpha accumulation and fibrosis in hypoxic adipose tissue, Br. J. Pharmacol. 173 (2016) 2001–2015.
[74] A. Takkikawa, A. Mahmood, A. Nawaz, T. Kado, K. Okabe, S. Yamamoto, A. Aminuddin, S. Senda, K. Tsuneyama, M. Ikutani, Y. Watanabe, Y. Igarashi, Y. Nagai, K. Takatsu, K. Koizumi, J. Imura, N. Goda, M. Sasahara, M. Matsumoto, K. Saeki, T. Nakagawa, S. Fujisaka, I. Usui, K. Tobe, HIF-1alpha in myeloid cells promotes adipose tissue remodeling toward insulin resistance, Diabetes 65 (2016) 3649–3659.
[75] D.A. Kane, E.J. Anderson, J.W. Price 3rd, T.L. Woodlief, C.T. Lin, B.T. Bikman, R. N. Cortright, P.D. Neufer, Metformin selectively attenuates mitochondrial H2O2 emission without affecting respiratory capacity in skeletal muscle of obese rats, Free Radic. Biol. Med. 49 (2010) 1082–1087.
[76] E. Fontaine, Metformin-induced mitochondrial complex I inhibition: facts, uncertainties, and consequences, Front. Endocrinol. 9 (2018) 753.
[77] A.K. Madiraju, Y. Qiu, R.J. Perry, Y. Rahimi, X.M. Zhang, D. Zhang, J.G. Camporez, G.W. Cline, G.M. Butrico, B.E. Kemp, G. Casals, G.R. Steinberg, D.F. Vatner, K. F. Petersen, G.I. Shulman, Metformin inhibits gluconeogenesis via a redox-dependent mechanism in vivo, Nat. Med. 24 (2018) 1384–1394.
[78] T. Yuan, J. Li, W.G. Zhao, W. Sun, S.N. Liu, Q. Liu, Y. Fu, Z.F. Shen, Effects of metformin on metabolism of white and brown adipose tissue in obese C57BL/6J mice, Diabetol. Metab. Syndrome 11 (2019) 96.
[79] P. Uhl, S. Pantze, P. Storck, J. Parmentier, D. Witizigmann, G. Hofhaus, J. Huwyler, W. Mier, G. Fricker, Oral delivery of vancomycin by tetraether lipid liposomes, Eur. J. Pharmaceut. Sci. 108 (2017) 111–118.
[80] I. Kurelac, N. Umesh Ganesh, M. Iorio, A.M. Porcelli, G. Gasparre, The multifaceted effects of metformin on tumor microenvironment, Semin. Cell Dev. Biol. 98 (2020) 90–97.
[81] Q. Liu, D. Tong, G. Liu, J. Gao, L.A. Wang, J. Xu, X. Yang, Q. Xie, Y. Huang, J. Pang, L. Wang, Y. He, D. Zhang, Q. Ma, W. Lan, J. Jiang, Metformin inhibits prostate cancer progression by targeting tumor-associated inflammatory infiltration, Clin. Cancer Res. 24 (2018) 5622–5634.